RSC Advances

ROYAL SOCIETY OF CHEMISTRY

www.rsc.org/advances

EBT anchored SiO_2 3-D microarray: A simultaneous entrapper of two different metal centers at High and Low oxidation states using its respective highest occupied and lowest unoccupied molecular orbital

Bhavya Srivastava, Milan K. Barman, Mousumi Chatterjee and Bhabatosh Mandal*

Analytical Laboratory, Department of Chemistry, Visva-Bharati,

Santiniketan 731235, India

*Author to whom all correspondence should be addressed: E-mail:

bhabatosh_mandal@yahoo.co.in

ABSTRACT:

A presto and facile synthesis of a mesoporous (Pore Diameter: 46.2-47.1 nm) material (FSG-EBT) through the immobilization of azo dye (EBT) on functionalizes silica gel (FSG) has been achieved. FSG-EBT simultaneously binds two different metal centers, Zr(IV) and Tl(I) respectively at their high and low oxidation states. Highest occupied molecular orbital (HOMO) of the extractor binds Zr(IV) with a breakthrough capacity (BTC) of 490 μmol g^{-1} and its lowest unoccupied molecular orbital (LUMO) extracts Tl(I) (BTC: 120 μmol g^{-1}). The LUMO has thus enhances BTC of the resin as a whole. This binding mode of sequence differs the earlier existing mode of binding, where, extractors bind metals using HOMO/ and LUMO operative on same metal centre only. HOMO/LUMO value (μmol g^{-1}) reiterates itself as a definite quantum mechanical descriptor of BTC and BTC is a definite descriptor of the state of metal (monomer/polymer) sorbed. Synthesis needs no stringent reaction condition like refluxing. Its corresponding nano material has been well assessed (composition: $[Si(OSi\equiv)_3(OH)\ .xH_2O]_n$[-Si$(CH_3)_2$-NH-$C_6H_4$-N=N-EBT]$_4$; Structure: tetrahedral) and reiterates by density functional theory (DFT) calculation. Along with its good extractor qualities [like high Pore Volume,

PV: 0.374689 cm^3 g^{-1}; Surface Area, SA: 330.968 m^2 g^{-1}; BTC (Q_0 = 476.7 μmol g^{-1}); Column efficiency, CE: 296 and Preconcentration Factor, PF: 120.20±0.04; reusability >1000 cycles; and faster rate of sorption-desorption], FSG-EBT possesses well demarcated spatial placement of HOMO-LUMO with a suitable band gap (η: 7.1471 eV). Here, HOMO-LUMO is well separated. It makes difficult for charge recombination by their mixing and shows its applicability as good donor-acceptor organic electronic device.

Keywords**:** Facile synthesis of FSG-EBT; DFT optimized resin; Simultaneous binder of high-low oxidation states; BTC =*f* (HOMO/ or LUMO); Photoelectronic properties.

1. INTRODUCTION

Trace level concentration and matrix effects [1] make it difficult to directly determine the analyte in real samples. So, a selective separation and preconcentration method for sample cleanup to obtain the trace-target-species in a small volume, prior to its detection/estimation by means of sophisticated instruments, is urgently required [2, 3]. In comparison with other techniques [4-13] with poor recovery and selectivity [14-16], solid phase extraction (SPE) creates much attention as it possesses many advantages. An appreciable selectivity and high values of preconcentration factors (PF) make SPE as an efficient method for proper sample clean up of an analyte. It creates attention because of its reusability, simplicity, and time-cost effectiveness [17]. More importantly, it needs low consumption of reagents and it is eco-friendly in nature [17-27]. Widely used solid phase (SP) sorbent, silica gel (SG), gets hydrolyzed at its working range of pH 7.5-8 [26]. Its lack of selectivity and irreversible nature of binding with metal ions confined its reusability also [23, 27-28]. Reported SP sorbents (like XAD resins, ion-exchange resin, cellulosic derivatives, and porous glass beads) [29-33] did not achieved appreciable selectivity to get the targeted species in its pure form by removing the interference of co-existing species. On the other hand, complicated method of synthesis, need of stringent stripping condition (1-3 mol L^{-1} HCl), low enrichment factor (PF: 20) [34] and their very

specific sorption qualities (every extractor is applicable for one or two selective metal ion only), ion-imprinted polymers (IIPs) [35, 36] cannot able to create much attention also. Consequently, Functionalized mesoporous silica gel (FSG) of versatile selectivity, having high surface area (SA), high pore volume (PV), high degree of mechanical and chemical stability, abilities for the faster and quantitative sorption at near neutral pH [6, 7], is urgently required. FSG may be synthesized by two traditional methods: (1) Impregnation of high molecular mass carboxylic acids (HMMLCE) on silanised silica gel (SSG) [17-22]. But here, during silanization, amidst SG, dichlorodimethylsilane (DMDCS), the cross-linker increases the size of SSG particles. Consequently, the surface activity (BET SA: 149.46 m^2g^{-1}; PV: 0.2001 mL g^{-1}) of the synthesized FSG in terms of sorption efficiencies was sharply decreased [17-22]. (2) In the second route, SG is chemically functionalized (grafted) using a suitable grafting component (like 3-aminopropyltrimethoxysilane, 3-Mercaptopropyltrimethoxy-silane, Chitosan) [23, 37, 38] to obtain FSG. Later, a selective chelating agent [viz., dithiozone, methylthiosalicylate, xylenol orange (XO), eriochrome black T (EBT), ethelenediaminetetra acetic acid, or 1-(2-Pyridylazo)-2-napthol (PAN) etc.] is chemically immobilized on this FSG. These chelating agents act as the selective metal trapping center and normally, the selectivity of the material appears as a function of solution pH. The chemical grafting protocols reported so far [3, 23, 37-47] are very much complicated (refluxing for more than 24h, need of several toxic / hazardous and costly chemicals like diethyl ether, pyridine, dichloromethane, Chloroacetyl chloride, 2-aminothiophenol, acetonitrile etc.), [25] time consuming (72-120 h) and sometimes it needs noble metal catalysts. These extractors were found to be unstable at both the high and low pH (pH 1-3 and 9.0) also. Moreover, low level of PF and poor selectivity (applied for synthetic binary mixtures) to remove the matrix effects restrict their uses in real samples. In addition to that, the cross-linking activities of the graftor (organosilicon compounds, chitosan or the traditional chlorosilanes) increase the size of the FSG

particles [23-24, 38-47] and as a result, their sorption activity in terms of SA (<300 m^2 g^{-1}) declines to a moderate level. Though in hydrosilylation reaction [45] grafting time has been reduced drastically it necessitates the use of costly and hazardous catalyst like tris(pentafluorophenyl)borane ($B(C_6F_5)_3$).

On critically analyzing these reports, to have the functionalized silica gel (FSG), we herein present for the first time a rapid (2-3 min) and room temperature grafting protocol for surface modification of amorphous silica gel (SG) using *m*-nitroaniline as the graftor. DMDCS has been used as a bridging component and the method needs no catalyst. Later, chemical immobilization of EBT on the FSG is made to obtain the extractor (FSG-EBT) of desired size, selectivity and stability [46]. It possesses O, N and S as the binding sites and consequently, a wide variety of metal ions having different hard-soft behavior (guided by η, a definite quantum mechanical descriptor) [48] can be adsorbed on it. The selectivity may be attained either by exploiting the differences in solution pH for extraction or through selective elution with the help of a selective eluent [17-22]. In an analytical application the resin has been utilized for necessary sample clean up [1, 49] of Th (IV) because of its essentiality and extensive application [50], toxicity and hazard (biological $T_{1/2}$ = 4 years, radioactive $T_{1/2}$= 1.4x 10^{10} years) [51]. A rigorous journey through the literature reveals that till date, extractors are able to extract either high or low oxidation states using their HOMO/ and LUMO operative on the same metal ion (viz., carbonyls, nitrosyls etc.) have been addressed [52]. However, HOMO and LUMO being far apart from one another, and thereby extracting two different metal centers respectively in their high and low oxidation states at the same time interval to enhance the breakthrough capacity (BTC) have yet not been reported. Besides the analytical usage, the photochemical applicability of the material as light emitting diode (LED) source or organic electronic device also merits mention. This is a genuine possibility because of its intra-molecular charge/hole transfer through donor-acceptor behavior (Scheme S1-S2). EBT, a water soluble azo dye reduced irreversibly by two-step one electron capturing process at –N=N- moiety (– 68

mV/s (EPc1) and at – 275 mV/s (EPc2) potentials) and the system dislikes to involve in charge recombination as is required in solar cells [53].

2. EXPERIMENTAL

***2.1 Reagents and chemicals*:** Unless otherwise stated, all chemicals and solvents used in this work were of analytical grade (BDH / E Merck, Bombay, India). Chemically bound Eriochrome black T (sodium 1-(1-hydroxy-2-naphthylazo)-2-naphthol-4-Sulphonate,BDH, Bombay, India), an water soluble azo dyes on silica gel (60-120 Mesh / 10-20 nm) was used as an ion extractor. Dimethyldichlorosilane (BDH, Bombay, India) was used a bridging component. Sn/HCl (E. Merck, Bombay, India) was used to reduce the nitro group to amine by usual method [54]. A standard stock solution of Th (IV) (0.01 mol L^{-1}), Zr(IV) (0.01 mol L^{-1}),U(VI) (0.01 mol L^{-1}) and Tl(I) (0.01 mol L^{-1}) were prepared by dissolving Th $(NO_3)_4$, $ZrO(NO_3)_2$, $UO_2(CH_3COO)_2 \cdot 2H_2O$ and $Tl_2(SO_4)$ (E. Merck, Bombay, India) in water and estimated complexometrically using XO indicator [2]. Buffer solutions of different pH were prepared from acetic acid (0.2 mol L^{-1}) and ammonium acetate (0.02 mol L^{-1}) in proper ratio (NH_4Cl: NH_3 = 17.3 g:142 mL L^{-1}). The aqueous solution of hexamine (BDH, Bombay, India) was used to adjust the pH of analyte solution.

2.2 Instrumentation: Most of the investigations have been performed on nano material. For the surface characterization of the extractor, the scanning electronic microscopy (SEM) was performed at 5.0 kV by using a Scanning Electron Microscope (JEoL JSM-6700-FESEM, ZEISS Supra 55). Prior to analysis, solid samples were sprinkled onto adhesive carbon tapes which were supported on metallic disks. SEM analysis (for normal sized material) was carried out on randomly selected points on the solid surfaces and back-scatter electron (BSE) detector was utilized during analysis. To have the particle sizes, the transmission electron microscopy (TEM) images were taken at an accelerating voltage 60-200KV in 50V steps using JEM-2100 microscope. To assess the probable composition of the ion-

exchange material, Energy Dispersive X-Ray Spectroscopy (EDX) was recorded on JEOL 2010 FEG microscope equipped with an EDX analyzer. The BET surface area and pore volume were determined by using automatic N_2 adsorption/desorption instrument Micromeritics ASAP 2020 V3.03 H (USA) at the instrumental conditions; Analysis Adsorptive: N_2 ; Analysis Bath Temperature: -195.850°C; measured warm free space 26.4410 cm^3 ; cold free space : 82.1653 cm^3 with sample mass 0.0810 g without thermal correction. The X-ray diffraction (XRD) patterns have been recorded on a Rigaku (Ultima IV) H-12 Japan (Kurary Co. Ltd. N) X-ray diffractometer in the 2θ measuring range at an angle of 0-90° with the scanning speed of 3° min^{-1} at room temperature by using Copper Kα ($\lambda = 1.5406 A^o$) as the scattering X-ray line source at a running condition of 40 kV and 30 mA. Fourier transform infrared (FTIR) spectra of extractor in its Th (IV) loaded and unloaded form were acquired on Shimadzu FTIR spectrophotometer (Model no. FTIR-8400S) using KBr pellets (Table S1). Measurements were taken in the wave number range from 400 to 4000 cm^{-1}. Raman spectra for the extractor and its Th(IV) loaded form was studied with Raman System RSLplus.R (Model no. : 3000 series) (Agiltron 15 Cabot Road, Woburn, MA 01801, USA) by irradiating the solid mass with 785 (S) nm laser source at the range of power input 90 -290 mW to achieve the precise resolution. The ^1H and ^{13}C NMR spectra of the corresponding nanomaterial (FSG and FSG-EBT) were recorded on NMR Bruker Ascend spectrometer (Model no. 400 MHz and 100 MHz for ^1H and ^{13}C respectively) relative to the solvent d_6-DMSO ^1H : δ = 4.79. Mass spectrometric data were obtained by using WATERS-Q-Tof-Premier-HAB213 and WATERS-Q-Tof-Premier-ESI-MS instruments. 2–5 µL of sample in DMSO and methanol (1:9) solvent was injected into the ionizing chamber and nitrogen gas was used for desolvation. Ionization protocols: capillary voltage: 3.5 kV; cone voltage: 30.0 V, extraction and ion guide voltages: 1.2 and 0.9 kV; source and desolvation temperature: 100 °C. The ESI-MS spectra were recorded at 1 s scans under positive full scan mode. The UV-Visible

spectra of the extractor (for the metal-ligand complexation at different mole ratio) were recorded on Shimadzu UV-Visible spectrophotometer (Model no UV-1800).The thermal stability and composition for the synthesized extractor and also the extracted Th(IV) species have been assessed by TGA/DTA analysis with PerkinElmer (STA 6000) Simultaneous Thermal Analyzer at the instrumental conditions viz., Flow-rate of Nitrogen: 20 mL/min , Working range of temperature: 40°C to 950°C with its rate of increment 25°C /min. Analytical applications of the material has been assessed with standard stock solutions of Th (IV) (0.01 mol L^{-1}), Zr(IV) (0.01 mol L^{-1}),U(VI) (0.01 mol L^{-1}) and Tl(I) (0.01 mol L^{-1}). The pH measurements were carried out with a digital Elico L1-120 pH meter combined with glass electrode.

2.3 Computational studies*:* Global hardness is a definite quantum mechanical descriptor and it is the cardinal index of chemical reactivity as well as stability of atoms and ions [3]. In order to perform the geometrical optimization and energy calculation of the FSG-EBT compound and to rationalize the physico-chemical behavior of the synthesized resin the proposed chemical structure of resin has been optimized by DFT method (Gaussian 09 Revision D.01 package). All the necessary calculations were carried out using B3LYP hybrid exchange-correlation functional STO-3G basis set [4].The global hardness of the extractor was determined from the energy of the HOMO-LUMO of the optimized structures. A series of DFT calculations of its building units have been made to judge the parallel shifting of both the electron density and hole within the molecular framework. The photoelectric properties has been assessed through density functional theory (DFT) and time dependent density functional theory (TDDFT) calculations in the Gaussian09 program package, with LSDA/SDD* functional and basis set.[4] In addition, neutral bond order (NBO) calculations of the optimized structures were performed to find the molecular orbital. The energies of the optimized structures were calculated after the ZPE (zero point energy) and thermal corrections.

2.4 Preparation of ion exchange material (FSG-EBT): Silica gel (A) (60-120 mesh/10-20 nm) and *m*-nitroaniline (B) were taken in toluene in a round bottom flask at 27^0C and dimethyldichlorosilane (DMDCS) (C) was added slowly at 300K. Here, *m*-nitroaniline binds with silica gel through DMDCS with the instantaneous formation of $(Si\text{-}O)_n\text{-}Si\ (Me)_2\text{-}NH\text{-}C_6H_4NO_2$ (D) (FSG). Subsequently, diazo salt (E) was made by using the literature method [55]. Finally, EBT was immobilized on this FSG by diazo coupling reaction and produces the resin (FSG-EBT) (F). The synthesized resin (deep black colored) mass was sequentially washed with 6 mol L^{-1} HNO_3. Finally, the Resin was washed with cold distilled water and dried at room temperature till constant weight. The whole synthesis (Scheme 1) need only 45-60 minutes. Each column could be used for at least 1000-1500 cycles without any loss of its exchange capacity.

A $\{(SiO_2)_n\text{-}O\text{-}H\}_4$ (SG) + B (*m*-nitroaniline (NA)) $\xrightarrow{DMDCS(C);-HCl}$ D ($\{(SiO_2)_n\text{-}O\text{-}\}_4[(Si\text{-}(Me)_2NH\text{-}\phi\text{-}NO_2]_4$) (FSG) $\xrightarrow{(i)Sn,HCl\,(ii)NaNO_2+HCl;0^oC-5^oC}$ E ($\{(SiO_2)_n\text{-}O\text{-}\}_4[(Si\text{-}(Me)_2NH\text{-}\phi\text{-}N{=}N^+]_4$) (Diazotized FSG) $\xrightarrow{EBT+NaOH}$ F ($\{(SiO_2)_n\text{-}O\text{-}\}_4[(Si\text{-}(Me)_2NH\text{-}\phi\text{-}N{=}N\text{-}EBT]_4$) (Resin)

Scheme 1: Synthesis of FSG-EBT [The termination of grafting can be easily identified through naked eye as it results an orange red colored material (FSG)]

2.5 Experimental Details for Analytical applications:

***2.5.1 Systematic studies for sample clean up*:** Rare Earth, Th(IV), in real samples (like alloys' and ore samples) is found to be present in a very low concentration. Th(IV) amidst several common cations/anions like Cl^- and SO_4^{2-} salts of Na^+, K^+, Ca^{2+} and Mg^{2+}, in the range of their natural contamination is also to be found in effluent samples. It needs an appropriate selective condition for extraction of Th(IV) on adsorbent and followed by its selective elution using an eluent of small

volume to obtain in enriched and pure state as well. Sorption of Th(IV), has been performed by both batch and column method.

2.5.2 Batch experiments: Sorption isotherms: 0.1 g of dry extractor was equilibrated with 50 mL of Th (IV) solutions of different concentrations (4×10^{-4}- 9×10^{-4} mol L^{-1}) at pH 6.5. The amount Th (IV) sorbed ($q_e = \frac{(C_i - C_e)\times V}{m}$ mg g^{-1}) in each solution was determined. In order to assess the applicability of the isotherms the correlation coefficient, R^2 and the RMSE ($\sqrt{[\frac{1}{n-2}\sum_{i=1}^{m}(q_e - q_{e(t)})^2}$; where, $q_{e(t)}$ is the theoretical estimate for corresponding q_e and n is the number of observations) were examined for the goodness-of-fit. The maximum R^2 and minimum RMSE indicate the applicability of the isotherm. The parameters for the batch experiment are given in Table S2.

2.5.3 **Column Experiments:** Batch experiment needs filtration in both extraction and elution steps to have the analyte. In the case of sample clean up from multicomponent mixtures some times needs repeatative filtration as well. On the other hand, column chromatograhy is an effective alternative for the sample clean up through separation and preconcentration to retrieve an analyte in its more enriched state [22, 27].

2.5.4 Extraction procedure: The chromatographic column (0.8 cm diameter) was packed with 1 g dry extractor to achieve a bed height of 2.5 cm. The pH of the column was adjusted at 6.5 using hexamine buffer. An aliquot containing 11.7 mL of Th(IV) (4×10^{-2} mol L^{-1}) in 20 mL hexamine buffer (pH 2.5-7.5) was passed through the column continuously till its saturation (498 μmol g^{-1}) at a flow rate of 2.0 mL^{-1} min at 27^0C to assess the effect of pH on extraction. The extraction reached equilibrium within a

few minutes. Increasing in the phase-mixing time up to 20 min had no significant effect on the extraction. Aqueous chemistry of Th (IV) is pH dependent [5, 6] and the conductance as well as the extraction is species dependent [7]. So, the systematic studies have also been made to investigate the effect of pH on conductance (mS) of aqueous Th (IV) solution at the said interval of pH. After extraction Th (IV) was stripped with 0.1 mol L^{-1} HNO_3 and the amount of Th(IV) in each fraction was determined complexometrically.

2.5.5 Effect of pH on extraction and conductance of Th (IV) solution: Extraction is pH dependent and Th (IV) exists as different species at different pH. Again, conductance is always species dependent. So, systematic studies have been made for both extraction and conductance at the range of pH 3.5-9.5 to assess the relationship of extraction and conductance.

2.5.6 Effect of foreign ions on extraction*:* Th(IV) in a pure sample was found to be extracted on the FSG-EBT surface and reached equilibrium quickly. Considering its analytical application in real samples, the extractability of Th(IV) was therefore systematically investigated in the presence of some commonly occurring ions [Na(I), K(I), Ca(II), Mg(II), Cl^-, SO_4^{2-}, ClO_4^-, NO_3^- up to 300 μg) and co-existing foreign ions like La(III), Ce(IV), Eu(III), Dy(III) in their natural contamination concentration (up to 0.5-5 μg L^{-1})[56] ranges (Table 1). Systematic studies of foreign ion stress on extraction of Th(IV) (sample volume: 50 mL) have been made by adding the foreign ions at constant flow-rate, analyte volume and temperature.

***2.5.7 Elution of Th(IV)*:** Systematic studies have been made on the elution behavior of Th (IV) with several acids of different concentrations (1.25×10^{-3}-500×10^{-3}(mol L^{-1})). Stripped Th (IV) was collected in several fractions (2 mL each) and estimated complexometrically using Xylenol Orange as

an indicator. 500×10^{-3}(mol L^{-1}) $HClO_4$ required least volume (5 mL) for the complete elution of Th(IV) and regarding its analytical convenience (identification and estimation) it was used to achieve the highest enrichment factor

($\frac{V_s}{12}\times \text{Recovery}(\%); V_s = sample\ \ Volume$) for sample clean up of the analyte (Table 2).

2.5.8 Break through capacity: For the determination of breakthrough capacity (BTC), 20 mL fractions of metal ion solution (10 μmol mL^{-1}) was passed through the column at an optimized pH (6.0) and effluent was collected, till the amount of metal ion concentration was the same in the feed and the effluent. A breakthrough curve was obtained by plotting the ratio $\frac{C_e}{C_0}$ against the effluent volume, where C_0 and C_e are the concentrations of the initial solution and effluent respectively. BTC is calculated using the formula ($\frac{C_0V(10\%)}{W}$), where C_0 is the concentration of the metal ion in mg mL^{-1}, V (10%) is the volume of the metal ion solution passed through the column when the exit amount reaches 10% of the initial amount (mg) and W is the weight of the extractor in g.

2.5.9 Optimization of preconcentration factor: The sample clean up of an analyte through preconcentration from a solution of large volume of relatively low concentration has an enormous implication in analytical chemistry. Preconcentration factor (PF) depends on the recovery and analyte volume. PF ($PF = \frac{C_f}{C_i}\times \text{Recovery}(\%)$) is product of the ratio of concentrations and the recovery of analyte. So, to assess the analytical performance of the synthesized extractor systematic studies have been made on the effect of sample size for the recovery of Th(IV). Effect of volume and concentration on

extraction has an inverse relationship on PF. So, its optimization has been made with respect to these two variables.

***2.5.10 Studies on the extraction of both high and low oxidation state*:** To investigate the sorption of both high and low oxidation states, the ion-exchange material was fully saturated with Zr (IV) (490 μmol g^{-1}), a cation which is stable in its high oxidation state (E_0 (ZrO^{2+}/Zr): -157) at a range of pH of 2.5 - 3.0. After that, an aliquot containing 12 mL of Tl(I) (10^{-2} mol L^{-1}), a species of low oxidation state in 20 mL hexamine buffer (pH 6.5-7.0) was passed through the column continuously to reach the saturation point (120 μmol g^{-1}). 0.01 mol L^{-1} HCl was used to stripe thallium as Tl(I), identified as a yellow ppt [8] of Tl_2CrO_4 with CrO_4^{2-} and subsequently Zr(IV) which is tightly bind at the exchange site, was eluted with the help of a strong eluent (≥ 2 mol L^{-1} HNO_3). Breakthrough value of the extractor for U(VI) and Tl(I) pair was found to be 522 and 127 μmol g^{-1} also. Tl(I) and U(VI) were eluted with 0.01 mol L^{-1}HCl and 0.05 mol L^{-1} H_2SO_4 respectively. Thus, there is no need to pay much attention on the extraction of single species of either high or low oxidation state.

3. RESULTS AND DISCUSSION

***3.1 Physicochemical characteristics of the extractor in terms of SEM, TEM, BET analysis*:**

The SEM micrographs of FSG-EBT (Figure 1a) confirm that the material is porous and the particle size is little bit irregular (approx. 110-150 μm) of almost of similar order of magnitude in both forms. It can also be noted that the surface of FSG-EBT is much cleaner than its Th (IV)-loaded form (Figure 1b). The size of the pure SG particles (60-120 Mesh, i.e., there are 100 (average) particles cm^{-1}) and the extractor s of both forms are in the same order (10^8 *pm*) in magnitude. The TEM and SEAD images (Figure 1c-d) of the corresponding

nanomaterial confirm that the size of the particle (12-24 nm) prevails within the size-range of nano SG (10-20 nm).

Usually DMDCS amid Si $(OH)_4$ enhances the size of SG by catenation through its cross linking (silanization [21, 22, 27]; equation 1). But here, being sandwiched between the SG and m-nitroaniline, it simply acts as a bridging component (Scheme 1) and becomes unable to promote catenation any further (equation 2). It suggests that as an end capping agent nitroaniline very efficiently impedes the process of cross linking.

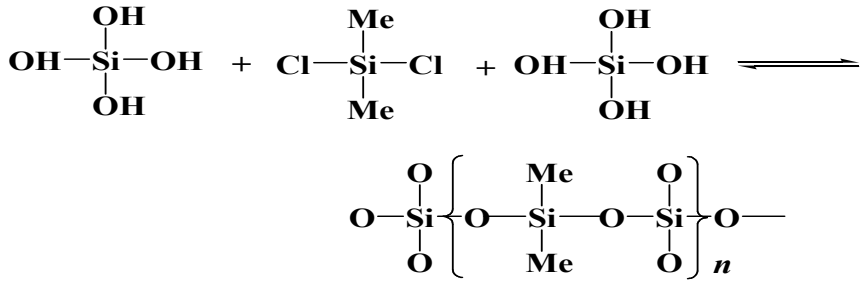

(1)

Equation 1: Silanization reaction; DMDCS amid Si (OH) 4 enhances the size of SG by catenation through its cross linking

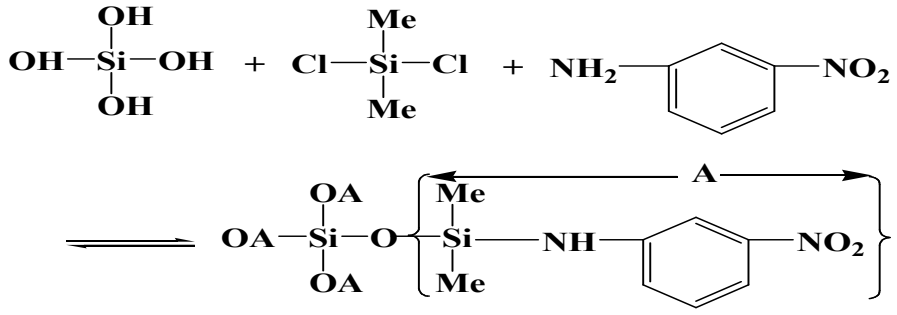

(2)

Equation 2: DMDCS being sandwiched between the SG and m-nitroaniline simply acts as a bridging component and becomes unable to promote catenation any further (eq. 2). m-nitroaniline group acts as the end capping group.

At P/P_0 0.0-1.0 FSG-EBT possesses high BET (Figure 1e) SA: 330.97 m^2 g^{-1}, PV: 0.388974 cm^3 g^{-1}, t-Plot micro PV: 0.007751 cm^3 g^{-1} and uniform pore size (width 47.0 A° / diameter 46.2 A°). The investigation confirms that the material is mesoporous in nature and its pore diameter lies below 50 A° ***(File-S1).***

3.2 TGA, EDX and XRD analysis to find out the composition of the extractor:

Amorphous SG appears to contain $\{Si(OSi\equiv)_3(OH).xH_2O\}_n$ [57]. TGA analysis of FSG-EBT (Figure 2a) exhibits three regions of weight loss. TGA endorses 8.8252 % of weight loss up to 100ºC for sorbed water molecules. In the 2nd step the weight loss by 0.7207% indicates removal of molecular water for the conversion of $\{Si[OSi]_{p=2-4}[OH]_{m=2-0}.xH_2O\}_n$ to $\{Si[OSi]_{p=2-4}[OH]_{m=2-0}\}_n$ polymer, and it continues up to 120ºC. Then the 3rd stage of weight loss begins and continues up to 800º C. The weight loss by 7.4239 % at the 3rd stage due to its thermal decomposition and leaves the residue of inorganic ash as $(SiO_2)_{4n+4}$ polymers. The probable composition of the synthesized resin is $[Si(OSi\equiv)_3(OH).xH_2O]_n[\text{-}Si(CH_3)_2\text{-}NH\text{-}C_6H_4\text{-}N{=}N\text{-}EBT]_4$ (Scheme-1) and the molecular mass of the moiety attached to the $[Si(OSi\equiv)_3(OH)]_n[\text{-}Si]_4$ framework is 2440. To account for 7.4239 % weight loss, the calculated value of n becomes 28. Weight loss at the second stage gives the value of *x* as 0.108. It yields the molecular mass (M) as 7.563×10^3 and so, 1 g resin can generates $\frac{1}{M}$ mol extractor (i.e., 132.2 µM g^{-1} HOMO or LUMO). These exchange sites (HOMO or LUMO) are able to extract 132.2 µmol g^{-1} or, 529 µmol g^{-1} of Th (IV) when it respectively exists as a monomer or tetramer. Comparing the TGA curves of the extractor in Th (IV)-loaded (Wt. loss: 8.8896 %) and unloaded forms (Wt. loss: 8.1500%) in the range of temperature 100-800ºC (Figure 2a), the difference in weight (0.7396 %) has been rationalized with the conversion of extracted Th (IV)-species into its inorganic ash containing $(ThO_2)_n$. It suggests the weight of the extracted species as 1064.16 g (equation 3) and reveals that a μ^2*O*-hydroxo tetramer, $[Th_4(OH)_8]^{8+}$ is present in the extractor as the sorbed species. This, in turn, suggests the breakthrough capacity of FSG-EBT for Th(IV) as 529 µmol g^{-1}.

$$\frac{W_{Th(IV)-species} - W_{(ThO_2)_n}}{W_{Th(IV)-species}} = 0.007517 \quad (3)$$

The calculated atomic composition (%) (Si: 25.90; O: 42.90; C: 25.0; Th: 0.89) obtained from TGA/DTA analysis and EDX (Figure 2b-c) values (Si: 20.60%; C: 29.49%; O: 49.68% and Th: 0.53%) reiterates the composition**,** $[Si(OSi\equiv)_3(OH)\,.xH_2O]_n[\text{-}Si(CH_3)_2\text{-}NH\text{-}C_6H_4\text{-}N{=}N\text{-}EBT]_4$ of FSG-EBT as well as the loaded extractor containing a μ^2O-hydroxo tetramer, $[Th_4(OH)_8]^{8+}$. The sorbed water molecules ($\frac{y \times H_2O}{M} g^{-1}$) generate a pore volume of ($\frac{51\times 18}{7563.00} mL\ g^{-1}$) 0.121380 mL g^{-1} and it attains 50% of the experimental (BET) values of 0.388974 mL g^{-1}. So, all the pores are not in proper sizes to intake water molecules. The XRD reflection patterns of FSG-EBT (Figure 2d), FSG-EBT containing both Zr(IV) and Tl(I) (Figure 2e) and amorphous silica gel (Figure 2f) exhibit a single broad peak respectively at 2θ = 22.38º, 21.92º and 22.0º. It clearly suggests the absence of any kind of long range ordering in the molecular network of FSG-EBT and its metal loaded form. Consequently, the amorphous identity of the precursor, SG (2θ = 22.0) (Figure 2f) was found to be retained in both the pure extractor and its metal loaded form. During the synthesis of FSG-EBT, reaction takes place at the outer surface of the central core [$\{(SiO_2)_n\text{-}O\text{-}\}_4$; having n=28] and retains the amorphous-identity as per the suggested reaction path (Scheme-1 and S3). It also reveals that the metal sorption process has no or little influence on the said central silica core. Here, the sorption of metal ions occur at the EBT moiety, present outside the silica core [$\{(SiO_2)_n\text{-}O\text{-}\}_4$.

***3.3 Structural identification of the resin in terms of FT-IR, RAMAN, NMR and MASS*:** The presence of various groups, viz., NO_2, -S=O & -OH in $–SO_3H$, -C-C- of Naphthalene ring, -N=N-, C-H of CH_3 in Si, aromatic C-H, O-H in SO_3H, N-H in (Si-N(H)-C(aromatic-ring)), O-H(phenolic), O-H in $Si(OH)_3$in the synthesized extractor have been characterized by comparing the experimental,

theoretical (DFT) and the reported peak positions in FT-IR / Raman spectra (together with the proposed assignments are summarized in Table S1) (Figure 3a-b). The predicted B3LYP/6−31G wave numbers are in consistently good agreement with the experimental FT-IR values. The presence of N-H in -Si-N(H)-Ar at 3525 cm^{-1} (reported: 3100-3500 and DFT: 3540.51) confirms linkage between silica moiety and nitroaniline. A nice correlation has been observed in the experimental (FT-IR (symmetric): 2400, 2616 cm^{-1}; FT-IR (asymmetric): 1800 cm^{-1}), DFT (FT-IR (symmetric): 2578cm^{-1}; FT-IR (asymmetric): 1710, 1855.09 cm^{-1}) and the corresponding reported values for -N=N- group (Table S1). It confirms the binding of azo-dye (EBT) with FSG. The strong FT-IR absorption band at 3697 cm^{-1} suffers a shift to 2980-3673 cm^{-1} as a broad peak in the Th(IV) loaded spectra, thereby confirming the presence of intramolecular H-bonding exists in μ^2*O*-hydroxo tetramer, $[Th_4(OH)_8(H_2O)_{16}]^{8+}$(Figure 3b). The Raman peak (Figure 3a) appears at 440 cm^{-1} (DFT) for -NH (attached to Si of DMDCS) is highly compatible with the experimental Raman spectral features (respectively 420 cm^{-1} and 421cm^{-1}in the extractor and its Th(IV) loaded forms) also (FigureS1), thereby confirming the formation of FSG. Si-O-Si linkage has been well characterized by the Raman band appears at 781cm^{-1} (DFT) and its experimental peak at 787,793 cm^{-1} (in both the loaded and unloaded forms).

The Raman peaks at 1800-1850 cm^{-1} (DFT) and 1800-1815cm^{-1} (experimental) confirms the presence of -N=N- groups in the synthesized material. The presences of aromatic rings have been well assessed by the Raman bands appear at 1200 cm^{-1} (DFT) and 1203 cm^{-1}(experimental) for aromatic C-C stretching vibration. Interestingly a new peak appears at 815 cm^{-1} in Raman spectra in Th (IV)-loaded extractor is in conformity with the presence of Th-O-Th in a μ^2*O*-hydroxo tetramer [58]. It agrees the TGA and EDX analysis. The ^{1}H (400 Mz) δ (ppm): 8.26 (1H, s, ArH), 8.19 (1H, s, ArH), 7.72 (2H, d, *J* = 4.8 Hz, ArH), 4.88 (1H, s, NH), 0.221 (6H, bs, CH_3) and ^{13}C NMR δ (ppm): [six aromatic

carbons: 148.48, 132.76, 131.36, 129.01, 123.20, 117.83 and two methyl carbons at Si: 30.32] spectra of intermediate D (the peaks found at lower and higher ranges are given in supplementary file: Figure S2) clearly confirm the attachment of *m*-nitroaniline to SG through DMDCS to functionalize the silica, (FSG). Now, turning to the behavior of the extractor molecule in terms of its experimental ^{1}H (400 Mz) δ (ppm): 7.044-8.135 (13 ArH); 2.161-2.430 (6H, CH_3) and ^{13}C [20 aromatic carbons: 121.01-148.40 with the shortage of 6 aromatic carbons due to probable symmetry properties of the molecule] NMR spectra (Figure S2 (c-f)), it is found that the experimental spectra are very much compatible with the DFT NMR signatures [^{1}H (400 Mz) δ (ppm): 13 ArH and ^{13}C: 26 aromatic carbons](Figure S2 (a-b)). The Electrospray Ionization-MS analysis shows six major fragments with m/z 694.5, 755.5, 813.5, 1103.5, 1159.3, 2126.5 resembling the fragmentation pattern (Figure 4a-f), of the extractor material. These fragmentation patterns reveal the attachment of different moieties ($(SiO_2)_n$, DMDCS, NH, EBT) and it confirms the reaction path (Scheme 1) for the synthesis of the extractor.

On the basis of these systematic investigations gave the composition of the synthesized resin as [Si $(OSi\equiv)_3(OH)$ $0.108H_2O]_{n=28}$ [-$Si(CH_3)_2$-NH-C_6H_4-N=N-EBT]$_4$ and its structural identification confirmed the 2D structure of the molecule also (Figure 5a).

***3.4 DFT analysis*:** The extractor has been synthesized from amorphous silica gel and it is a high molecular mass polymeric material. As a result of which single crystal XRD analysis was beyond of our scope to have the three dimensional structure of the material. So, density functional theory calculations have been performed on this 2D structure (Figure 5a) to obtain the 3D optimized structure of this material. All DFT [59] calculations have been made by using STO-3G basis set with B3LYP/6 hybrid function to have the optimized structure (Figure 5b) and its global hardness was calculated from the resulting HOMO-LUMO band gap. In the DFT optimized molecule (Figure 5b), four EBT moieties are attached at the four

tetrahedral corners (leveled as 2nd, 3rd, 4th, 5th O) of the central Silicon (1st Si) through the linker component (substituted m-diazaniline group) and the bridging component (DMDCS). The optimized compound possesses high degrees of dipole moment (6.7214 Debye). At any time interval, HOMO (-5.7675 eV) is suitably located at only one m-diazaniline part (slightly defused to dimethyl group of DMDCS) moiety out of four, while LUMO (3.2431 eV) is highly localized on the region having m-diazaniline moiety and one naphthol ring of EBT moiety. During optimization it is found that HOMO and LUMO are present at two different edges of the tetrahedra (Figure 6a-e) with a suitable photosensitized level of HOMO-LUMO band gap, 7.1471 eV. With passage of time, both HOMO and LUMO which were initially present at two different edges of the tetrahedra, change their positions. They do this preferably instead of clustering at the same edge of the tetrahedra or overlapping each other (Figure 6a-e). As a result of which the process of charge recombination is denied. This, undoubtedly, increases the life time of the ejected photoelectron to increase the solar efficiency (as per Scheme S1-S2) [60-62].

Considering the symmetry properties of the molecule only one tetrahedral edge of FSG-EBT was taken as a model compound (Figure S2c) to have the NMR spectra from DFT calculation. Thus the NMR fingerprint (Figure S2, S3) generates a full poof molecular identity of the extractor material at its convincing level (Figure 5a-b). The theoretical UV-Vis spectra (two major peaks at 699.4 and 432.2 nm; (Figure S4), obtained by TD-DFT optimization of the extractor, is highly compatible with the experimental UV-Vis spectral features (two major peaks at 578 and 450 nm) and reiterates the molecular structure of the extractor. The experimental spectral positions (274, 366.4, 450, 578, 880.5, 950.3 and 1094.5 nm) (Figure 7a-b) are nearly compatible and support the transfer of hole by hopping mechanism (Figure S5). Presence of both HOMO and LUMO in the same molecule (Figure S5) with a clean demarcation makes it a prolific candidate to be used as a donor-acceptor organic electronic device [62]. We hope to explore

this aspect in near future. Now, turning to its metal binding abilities, the theoretical ground reality reveals that metal ion in its higher oxidation state may bind through HOMO while LUMO being far apart from HOMO (7.1471 eV), placed at the other part of the molecule would have been involved in the binding of metal in its lower oxidation state.

3.5 Analytical application of the synthesized Resin in terms of Th(IV), Zr(IV), U(VI) and Tl(I):

3.5.1 Analysis of the Sorption isotherm: Plot of $C_e(\mu M\ \ g^{-1})$ vs. $C_e/q_e\ (g\ \ mL^{-1})$ gives a linear relationship (Figure S6) ($y = 0.00904x + 0.00117;\ R^2 = 0.98928$) with a slope of 0.00904 which generates the Q_0 as 110.6195 mg g^{-1}(i.e., 476.7 µM g^{-1}) and b (energy parameter of adsorption) was found to be 7.7265 L g^{-1} respectively. The very high energy parameter (Langmuir b: 7.7265 L g^{-1}) suggests high affinity of the adsorbent towards the adsorbate and excellently justifies the faster rate of equilibration (< 1.0 minutes). The higher RMSE (0.9636) and poor Freundlich binding parameter for physi-sorption (n: 1.61) (Table S2) also denies multi-layer formation (Figure S3).

3.5.2 Effect of pH on extraction and conductance: pH of the influent solution is an important controlling parameter in the sorption process [63, 64]. The pH–extraction and pH-conductance relationships (Figure 8) clearly indicate the presence of different kinds of Th(IV) species exist at different range of pH. The retention (mg g^{-1}) increases with the increase in pH (a-d), reaches a maximum at the pH range 6.5-7.5 and then decreases (d-e) with further increase in pH. The studies show that there is a sharp jump (b-c) for extraction at the moderate range of pH, 4.5-5.25. The systematic studies for conductance of the analyte solution at the prevailing range of pH and

concentration (4×10^{-2} mol L^{-1} of Th(IV) in 20 mL hexamine buffer (pH 2.5-7.5)) show a gradual decrease in both the initial (a-b) and final part (c-d) of the pH-conductance relationship (Figure.8) with a similar type of sharp sigmoid jump at pH axis (b-c) like pH-extraction relationship. This clearly approves the change of analyte species from one to another according to the change of pH from 4.5 to 5.25. Further enhancement of pH at the short interval may increase the population of that species causing a gradual rise up to its limiting values reaching pH 7.0±0.25. The problem of hydrolysis comes in to the play with further increase of pH and we observe noticeable depletion in the extent of extraction at the time-pH-extraction relationship (Figure 8a). At the initial part of the pH-extraction relationship, the gradual up rise is reflected by the existing species having low level of affinity towards the exchange site resulting in a poor extraction (confined to 30% only). Affinity between the acid (Th(IV)) and Base (exchanger) is guided by the definite quantum mechanical descriptor, viz. the hardness, η.

3.5.2 Effect of Common cations/anions and flow-rate on extraction: The systematic extraction chromatographic studies on Th(IV) ensured its quantitative extraction at the optimum pH 7.0 ± 0.5 (Figure 8a). Common cations/anions (Cd^{2+}, Mg^{2+}, Zn^{2+}, Ni^{2+}, Na^{+}, K^{+}, SO_4^{2-}, ClO_4^{-}, CH_3COO^{-} and NO_3^{-} up to 250 µg), co-existing lanthanide ions (like La(III), Ce(IV), Dy(III) and Eu(III) up to 5µg L^{-1}) and flow rate up to 2.5 mL min^{-1} did not interfere (Table 1) the sorption of Th(IV). The recoveries (%) of Th(IV) were quantitative (> 91%) and the analytical performance of extractor with respect standard deviation (< 0.05) was found to be good. At low pH (< 5.0), the otherwise difficult deprotonation of FSG and solubility of Th (IV) gave its poor sorption [27].

3.5.3 Breakthrough capacity: The analyte concentration in effluent was close to 10% to that of the background level up to passage of 49.8 mL (0.01 mol L^{-1}) Th (IV) solution (Figure 9a) and it attains BTC at 498 µmol g^{-1} of dry extractor. Now turning to its surface behavior, FSG-EBT sorbs the analyte as a monolayer on its external surface (Langmuir: Figure S6). The determined Q_0 corroborates the breakthrough value (498 µmol g^{-1}) and suggests the chemisorptions of Th (IV) as a tetramer (TGA: 527 µmol g^{-1}) at the exchange site. It is also comparable to the TGA (527 µmol g^{-1}). At a fixed amount of Th (IV) the volume-recovery relationship yields two desorption constants (k^1: 2×10^{-3} and k^2: 9.6×10^{-2} and PF (Figure 9b) gets optimized [2, 17, 22] at their points of intersection with a value of 120.20 ± 0.04 (Figure 9 b-c).

3.5.4 Extracted species: The distribution of Th (IV)-species depends on the level of pH, the total Th (IV) concentration, and the ratio (n) of $\frac{[OH^-]}{[Th^{4+}]}$ in the complex [65]. μ^2*O*-hydroxo dimer, $[Th_2(OH)_2(H_2O)_{12}]^{6+}$ is found to be present at n = 1 while the polymeric species a μ^2*O*-hydroxo tetramer, $[Th_4(OH)_8(H_2O)_{16}]^{8+}$, and a μ^3*O*-oxo hexamer, $[Th_6O_8(H_2O)_n]^{8+}$) at n > 2.0 [63]. It has also been observed that at pH > 2.9 and concentration of Th(IV) > 10^{-3} M both of them are the prime contributors [63-69]. In our study at its prevailing conditions (pH: 6.5, $[Th^{4+}]$: $10^{-2} mol\ L^{-1}$ and $\frac{[OH^-]}{[Th^{4+}]}$: $10^{-5.5}$) the maximum sorption of Th (IV) becomes 498 µmol g^{-1} (FSG: Th(IV) = 1:4) and corroborates TGA: 527 µmol g^{-1} and Langmuir: 476.7 µmol g^{-1} values (Table:S2). In the UV-visible spectra (Figure 10) the absorbance maxima at 424.6 nm for pure extractor (nano form) in DMSO has been totally removed at a mole ratio of 1:4 (extractor: Th (IV) and reiterates the sorption ratio. Now, at any particular time interval HOMO, entitled to bind Th (IV) by electron donation, exists at one edge of the tetrahedra of the resin (Figure 11a) (DFT). This in turn indicates that Th (IV) exists as its

tetramer (at pH 6.5 and [Th^{4+}]: $10^{-2} mol\ L^{-1}$) in the vicinity of HOMO in extractor -metal complex (Figure 11b).

***3.5.5 Simultaneous Sorption of both the high and low oxidation state*:** In the prevailing condition for extraction (pH: 6.5 and [Zr (IV)]: 10^{-2} mol L^{-1}), both the tetranuclear $[Zr_4(OH)_8(H_2O)_{16}]^{8+}$ and octanuclear $[Zr_8(OH)_{20}(H_2O)_{24}]^{12+}$ species of Zr(IV) are present in equilibrium [61].The compatibility of breakthrough value of Zr(IV) (490 µmol g^{-1}) with Langmuir (Q_0: 476.7 µmol g^{-1}) and TGA (527 µmol g^{-1}) indicates the ratio of HOMO: metal as 1:4. So, Zr(IV) is present as a tetramer. DFT calculations produce a symmetric LUMO core within the tetrameric entity of tetranuclear $[Zr_4(OH)_8(H_2O)_{16}]^{8+}$ which efficiently makes a bond with HOMO of FSG-EBT (Figure 12). Now, after attaining BTC [i.e., when HOMO is totally blocked with Zr(IV)], Tl(I) (an electron rich species) is forced to move towards LUMO (Figure 12) of FSG-EBT to make its synergistic attachment as a monomer (BTC: 120 µmol g^{-1}) by back donation in presence of a very stable and poor oxidizer Zr(IV) (E_0 (ZrO^{2+}/Zr): -157).

Thus, both the metal ions rarely and remarkably exist in two different spatial locations of FSG-EBT at their high and low oxidation states (Figure 12) keeping intact the core identity of the extractor (XRD results; Figure 2e). The behavior was tested with Th(IV), U(VI) and Ti(IV), (elements of transition series) and the result [518, 522 and 260 µmol g^{-1} for Th(IV), U(VI) and Ti(IV) along with 124-128 µmol g^{-1} Tl(I)] shows remarkable agreement with the simultaneous sorption abilities for high and low oxidation states of the extractor at its respective HOMO-LUMO levels. Here, at the prevailing condition for extraction (pH: 6.5 and [Ti (IV)]: $10^{-2} mol\ L^{-1}$), Ti(IV) exists as a dimer [27] while both Th(IV) and U(VI) are reported to exists as tetramer [61, 65]. However, in the reverse sequence of

sorption, thallium in its stable Tl(I) form cannot appreciably attack the less electronegative LUMO of the pure extractor (8-10 μmol g^{-1}). The sorption of Tl(I) at LUMO was slow (equilibration time: 10 minutes) probably because of the rapid change in position of LUMO from one tetrahedral edge to another. The sorption of metal ions [Th(IV), Zr(IV), U(VI) and Ti(IV)] with other extractors (FSG-X; where, X's were EBBBB, NV, GNV, PAN) was found to be a integral multiple of HOMO/LUMO values (μmol g^{-1}) (Table 4).

***3.5.6 Effect of desorption condition and repeated use*: T**he sorption of Th(IV) on the Resin was very low below pH 1.5. So, systematic studies on its elution were made with different acid solutions of various concentrations (10×10^{-3} – 2000 $\times10^{-3}$ mol L^{-1}) (Table 2). These results indicate that 500 $\times10^{-3}$ (mol L^{-1}) $HClO_4$ (5 mL) is sufficient for quantitative elution for Th(IV) (Figure S7) and it yields a good column efficiency (CE) in terms of plate number (N: 296) [22]. To investigate the reusability of the Resin, the sorption and desorption cycles were repeated 800-1000 times by using the same adsorbent and BTC was decreased by only 0.2-0.3%.

3.5.7 Optimization of preconcentration factor: Systematic studies have been made on the extraction and recovery of of Th (IV) (1 mL solution of 0.01 $molL^{-1}$) with respect to influent volume of different sample sizes (100-1200 mL). Plot of influent volume vs recovery (%) yields two linear segments (Figure 9b) ($y=-0.002x+99.65; R^2=0.992$ and $y=-0.096x+150.7; R^2=0.947$) intersecting at a volume of 600 mL. The slopes of the corresponding segments are the desorption efficiencies and yielded the desorption constants [9] $K^1_{Desorption}(2\times10^{-3})$ and $K^2_{Desorption}(9.6\times10^{-2})$. Up to 600 mL the recoveries were quantitative (≥97

%) and then it decreases gradually. During sample clean up (extraction followed by stripping with 5 mL 0.5 mol L^{-1} $HClO_4$), the analyte solution containing Th(IV) is always confined to small volume (5 mL). At the initial stage of quantitative range of recovery, the first term ($\frac{V_{\inf luent}}{V_{effluent}}$) of P.F. (equation 4) predominates. This promotes sharp increase of the enrichment factor and consequently improves the analytical detection limit. However, enrichment factor gradually decreases due to its poor recovery ($K^{2}_{Desorption} >> K^{1}_{Desorption}$) at a higher dilution (volume effect) [9] and the value was optimized at 120.2 ($y = -0.096x + 150.7; R^2 = 0.947$) at an influent volume of 640 mL (Figure 9c).

$$\text{P.F.} = \frac{V_{\inf luent}}{V_{effluent}} \times \text{Recovery}(\%) \quad (4)$$

3.5.8 Analytical performance in comparison to other matrices: The sorption process on FSG-EBT follows the Langmuir adsorption isotherm with a high adsorption coefficient Q_0 110.6195 mg g^{-1}(i.e., 476.7 µmol g^{-1}) and high energy parameter of adsorption (b: 7.7265 L g^{-1}). Q_0 indicates the amount of Th(IV) for the monolayer saturation and it represents the adsorption capacity (i.e., BTC, 498 µ mol g^{-1}) of the ion-exchange material. The value of this adsorption capacity (476.7-498 µmol g^{-1}) (Table-3) is comparable to that of other matrices. On the other hand, the BET surface area (330.97 m^2g^{-1}) of the present extractor is also found to be comparatively much higher than earlier reported functionalized silica gel sorbents (FSG-Xs: 125-149 m^2g^{-1}) for Th(IV) uptake [27,28,36]. In addition to that, the present extractor binds a second metal centre (Tl(I), a low oxidation state) utilizing its LUMO, present at a different spatial location. Thereby, increase the BTC by an amount of 120 µmol g^{-1}, which may be enhanced up to 498 µmol g^{-1}, the HOMO level BTC value.

4. CONCLUSIONS: In comparison to other matrices (Table-3), we herein for the first time report three important outcomes as follow:

1) An efficient (yield: 99%, at room temp), rapid (2-3 minutes), metal-free catalytic and green (in view of some commonly available solvents/chemicals in a very simple laboratory set up and without the involvement of complicated steps with stringent reaction conditions) grafting protocol, recognizable through naked eye. The material has been well characterized (composition: $[Si\ (OSi\equiv)_3(OH).\ xH_2O]_n[\text{-}Si(CH_3)_2\text{-}NH\text{-}C_6H_4\text{-}N{=}N\text{-}EBT]_4$ and structure: tetrahedral) and it is further corroborated by standard DFT calculations. TGA was found to be sufficient to elucidate the composition of this kind of material. More advantageously, the corresponding nanomaterial gives well-characterized NMR signals in solution phase and rules out any need of solid phase NMR. The material is mesoporous with uniform pore size (pore width 47.0 A° / pore diameter 46.2 A°).

2) With respect to other matrices (Table-3), along with its analytical performances [high BET SA (330.968 m^2), high BET PV (0.388974 $cm^3\ g^{-1}$), high BTC (490-527 µmol g^{-1}), reusability (up to 500-800 cycles), high PF: 120.20±0.04), inertness (chemically: up to 6 mol L^{-1} HNO_3, 8 mol L^{-1} HCl, 6 mol L^{-1} H_2SO_4 and thermally: 320 ºC (mp)] *it uniquely binds two metal centers,* Zr(IV)/U(VI)/Ti(IV) and Tl(I), in their high and low oxidation states simultaneously at its respective HOMO and LUMO which are spatially separated (Scheme 2a). Thus, it differs from the earlier existing materials reported so far in an important aspect. The aspect includes stabilization of high (transition metal complexes having ligands like IO_6^{5-}) [69] and low (carbonyls) [52, 70] oxidation states of metals (Scheme 2b).

3) The number and nature of exchange sites (e.g., phenolic -OH, $-SO_3H$ or $-NO_2$) of the extractor are not the determining parameters for metal binding (BTC) but it is the availability of HOMO/LUMO or its integral multiple value (n× HOMO/LUMO µM g^{-1}) that capture them in their high/low oxidation state. *So, HOMO/LUMO value is a definite quantum mechanical descriptor of BTC and BTC is a definite descriptor of the state of the metal (monomer, dimer, trimer, tetramer, etc.) sorbed.* Two different BTC for metal sorption in their high and low oxidation states may be

obtained when the HOMO and LUMO are well placed at two different spatial locations in the extractor. The classical BTC (saturation of HOMO) of FSG-EBT is sufficiently high (490-527 μmol g^{-1}) (Table-4) and has been enhanced by 120 μmol g^{-1} for Tl(I) utilizing its LUMO, which even may be enhanced up to 490-527 μmol g^{-1} (the HOMO value). The analytical performances were found to be poor in its corresponding nanomaterial. In addition to above other two features include; i) TGA was found to be enough to elucidate the composition of this kind of exchange material. ii) And its corresponding nanomaterial gave well-characterized NMR signals in solution phase and ruled out any need of solid phase NMR.

5. Acknowledgment: The authors are grateful to Laboratoire CRISMAT, UMR 6508, CNRS/ ENSICAEN, Caen Cedex, France, for experimental assistance for EDX, SEM and Department of physics, Visva Bharati for XRD, RAMAN for partial assistance research grant to carry out the research work.

ASSOCIATED CONTENT: Supporting information.

6. REFERENCES:

[1] A. Walcarius and L. Mercier, Mesoporous organosilica adsorbents: nanoengineered materials for removal of organic and inorganic pollutants, *J. Mater. Chem.*, 2010, **20**, 4478-4511.

[2] B. Mandal and N. Ghosh, Extraction chromatographic method of preconcentration and separation of lead (II) with high molecular mass liquid cation extractor , *Desalination*, 2010, **250**, 506-514.

[3] T. Yordanova, P. Vasileva, I. Karadjovaa and D. Nihtianovac, Submicron silica spheres decorated with silver nanoparticles as a new effective sorbent for inorganic mercury in surface waters, *Analyst*, 2014, **139**, 1532-1540.

[4] T. V. Hoogerstraete, B. Onghena and K. Binnemans, Homogeneous Liquid–Liquid Extraction of Metal Ions with a Functionalized Ionic Liquid, *J. Phys. Chem. Lett.*, 2013, **4**, 1659–1663.

[5] T. S. Anirudhan and S. R. Rejeena, Thorium(IV) Removal and Recovery from Aqueous Solutions using Tannin-Modified Poly(glycidylmethacrylate)-Grafted Zirconium oxide Densified Cellulose, *Ind. Eng. Chem. Res.*, 2011, **50**, 13288–13298.

[6] S. B. Uktiryaki, R. Say, A. Ersoz, E. Birlik and A. Denizli, Selective preconcentration of Thorium in the presence of UO_2^{2+}, Ce^{3+} and La^{3+} using Th(IV)-imprinted polymer, *Talanta*, 2005, **67**, 640-645.

[7] T. Prasada Rao, R. Kala, S. Daniel, Metal ion-imprinted polymers-Novel materials for selective recognition of inorganics, *Anal. Chim. Acta*, 2006, **578**, 105-116.

[8] S.H. Lee, J. La. Rosa, J. Gastaud and P. P. Povinec, The development of sequential separation methods for the analysis of actinides in sediments and biological materials using anion-exchange resins and extraction chromatography, *J. Radional. Nucl. Chem.*, 2005, **263**, 419-425.

[9] E. Constantinou and I. Pashalidis, Thorium determination in water samples by liquid scintillation counting after its separation by cloud point extraction, *J. Radioanal. Nucl. Chem.*, 2011, **287**, 261-265.

[10] V.K. Jain, A. Handa, S.S. Sait,P. Shrivastav, Y.K. Agrawal, Pre-concentration, separation and trace determination of lanthanum(III), cerium(III), thorium(IV) and uranium(VI) on polymer supported o-vanillinsemicarbazone, *Anal. Chim. Acta*, 2001, **429**, 237–246.

[11] S. Panja, P. K. Mohapatra, S. C. Tripathi and V. K. Manchanda, Transport of Thorium(IV) Across a Supported Liquid Membrane Containing N,N,N′,N′-Tetraoctyl-3-oxapentanediamide (TODGA) as the Extractant, *Sep. Sci. Technol.*, 2010, **45**, 1112-1120.

[12] V.N. Zaitsev, L.S. Kostenko, N.G. Kobylinskaya, Acid–base properties of silica-based ion-extractor having covalently bonded aminodi(methylphosphonic) acid, *Anal. Chim. Acta*, 2006, **565**, 157-162.

[13] H. H. P. Yiua and P. A. Wright, Enzymes supported on ordered mesoporous solids: a special case of an inorganic–organic hybrid, *J. Mater. Chem*., 2005, **15**, 3690–3700.

[14] C. Pin, J. F. S. Zalduegui, Sequential separation of light rare-earth elements, thorium and uranium by miniaturized extraction chromatography: Application to isotopic analyses of silicate rocks, *Anal. Chim. Acta,* 1997, **339**, 79-89.

[15] Z. Wei, H. Zhao, J. Zhang, L. Deng, S. Wu, J. He and A. Dong, Poly(vinyl alcohol) electrospun nanofibrous membrane modified with spirolactam–rhodamine derivatives for visible detection and removal of metal ions, *RSC Adv.*, 2014, **4**, 57522-57528.

[16] G. V. K. Puvvada, Liquid-Liquid extraction of gallium from Bayer process liquor using Kelex 100 in the presence of surfactants, *Hydrometallurgy*, 1999, **52**, 9-19.

[17] B. Mandal, U.S. Roy, D. Datta, N. Ghosh, Combined cation-exchange and extraction chromatographic method of pre-concentration and concomitant separation of Cu(II) with high molecular mass liquid cation extractor after its online detection, *J. Chromatogr. A.*, 2011, **1218**, 5644-5652.

[18] P. M. Price, J. H. Clark and D. J. Macquarrie, Modified silicas for clean technology, *J. Chem. Soc., Dalton Trans.*, 2000, 101-110.

[19] C.F. Poole, New trends in solid-phase extraction, *Trends Anal. Chem.*, 2003, **22**, 362-373.

[20] E. P. Horwitz, M. L. Dietz, R. Chiarizia, H. Diamond, S. L. Maxwell III and M. R. Nelson, Separation and preconcentration of actinides by extraction chromatography using a supported liquid anion extractor : application to the characterization of high-level nuclear waste solutions, *Anal. Chim. Acta*, 1995, **310**, 63-78.

[21] R. Antony, S. T. D. Manickam, P. Kollu, P. V. Chandrasekar, K. Karuppasamy and S. Balakumar, Highly dispersed Cu(II), Co(II) and Ni(II) catalysts covalently immobilized on imine-modified silica for cyclohexane oxidation with hydrogen peroxide, *RSC Adv.*, 2014, **4**, 24820-24830.

[22] B. Mandal and N. Ghosh, Combined Cation-Exchange and Extraction Chromatographic Method of Pre-concentration and Concomitant Separation of Bismuth (III) with High Molecular Mass Liquid Cation extractor , *J. Hazard. Mater.*, 2010, **182**, 363-370.

[23] M. Zougagh, L J. M. C. Pavon, A. Torres and D. Gracia, Chelating sorbents based on silica gel and their application in atomic spectrometry, *Anal. Bioanal. Chem.*, 2005, **38**, 1103-1113.

[24] B. Y. Spivakov, G. I. Malofeeva and O. M. Petrukhin, Solid-phase extraction on alkyl-bonded silica gels in inorganic analysis, *Anal. Sci.*, 2006, **22**, 503-519.

[25] F. A. Aydin and M. Soylak, Solid phase extraction and preconcentration of uranium (VI) and thorium(IV) on Duolite XAD761 prior to their inductively coupled plasma mass spectrometric determination, *Talanta*, 2007, **72**, 187-192.

[26] D. B. Gazda, J. S. Fritz and M. D. Porter, Multiplexed Colorimetric Solid-Phase Extraction: Determination of Silver (I), Nickel (II), and Sample pH, *Anal. Chem.*, 2004, **76**, 4881-4887.

[27] M. K. Barman, B. Srivastava, M. Chaterjee and B. Mandal, Solid phase extraction, separation and preconcentration of titanium (IV) with SSG-V10 from some other toxic cations: a molecular interpretation supported by DFT, *RSC Adv.*, 2014, **4**, 33923-33934.

[28] R. R. Bhatt and B. A. Shah, Sorption studies of heavy metal ions by salicylic acid–formaldehyde–catechol terpolymeric resin: Isotherm, kinetic and thermodynamics, *Arab. J. Chem.*, 2015, **8**, 414-426.

[29] X. B. Zhu, X. J. Chang, Y. M. Cui, X. J. Zou, D. Yang and Z. Hu, Solid-phase extraction of trace Cu(II) Fe(III) and Zn(II) with silica gel modified with curcumin from biological and natural water samples by ICP-OES, *Microchem. J.*, 2007, **86**,189-194.

[30] M. R. Buchmeiser, G. Seeber and R. Tessadri, Quantification of Lanthanides in Rocks Using Succinic Acid-Derivatized Sorbents for On-Line SPE-RP-Ion-Pair HPLC, *Anal. Chem.*, 2000, **72**, 2595-2602.

[31] P. Z. Ray and H. J. Shipley, Inorganic nano-adsorbents for the removal of heavy metals and arsenic: a review, *RSC Adv.*, 2015, **5**, 29885-29907.

[32] G. Z. Fang, J. Tan and X.P. Yan, An Ion-Imprinted Functionalized Silica Gel Sorbent Prepared by a Surface Imprinting Technique Combined with a Sol-Gel Process for Selective Solid-Phase Extraction of Cadmium(II), *Anal. Chem.*, 2005, **77**, 1734-1739.

[33] D. Troegel, T. Walter, C. Burschka and R. Tacke, Synthesis and Characterization of Tris(mercaptomethyl)(2,4,6-trimethoxyphenyl)silane and Its Use for the Immobilization of the $Si(CH_2SH)_3$ Group on Silica via an Si-O-Si Linkage, *Organometallics*, 2009, **28**, 2756-2761.

[34] C. Lin, H. Wang, Y. Wang and Z. Cheng, Selective solid-phase extraction of trace thorium(IV) using surface-grafted Th(IV)-imprinted polymers with pyrazole derivative, *Talanta*, 2010, **81**, 30-36.

[35] Y. Zhai, D. Yang, X. Chang, Y. Liu and Q. He, Selective enrichment of trace copper (II) from biological and natural water samples by SPE using ion-imprinted polymer, *J. Sep. Sci.*, 2008, **31**, 1195-1200.

[36] Q. He, X. J. Chang, Q. Wu, X. P. Huang, Z. Hu and Y. H. Zhai, Synthesis and applications of surface-grafted Th(IV)-imprinted polymers for selective solid-phase extraction of thorium(IV), *Anal. Chim. Acta*, 2007, **605**, 192-197.

[37] M. E. Mahmoud, Silica gel-immobilized Eriochrome Black-T as a potential solid phase extractor for Zinc (II) and magnesium (II) from calcium (II), *Talanta*, 1997, **45**, 309-315.

[38] J. Roosen, J. Spooren and K. Binnemans, Adsorption performance of functionalized chitosan–silica hybrid materials toward rare earths, *J. Mater.Chem. A*, 2014, **2**, 19415-19426.

[39] F. Hoffmann, M. Cornelius, J. Morell and M. Froba, Silica-Based Mesoporous Organic–Inorganic Hybrid Materials, *Angew. Chem.Int. Ed.*, 2006, **45**, 3216-3251.

[40] N. Wang, Y. Guo, L. Wang, X. Liang, S. Liu and S. Jiang, Preparation of an aminopropyl imidazole-modified silica gel as a sorbent for solid-phase extraction of carboxylic acid compounds and polycyclic aromatic hydrocarbons, *Analyst*, 2014, **139**, 2531-2537.

[41] E. F. Vansant, P. V. D. Voort and C. Vrancken, *Studies in Surface Science and Catalysis*; Elsevier Amsterdam, Part II, 1995, 194-198.

[42] T. Shimada, K. Aoki, Y. Shinoda, T. Nakamura, N. Tokunaga, S. Inagaki and T. Hayashi, Functionalization on Silica Gel with Allylsilanes. A New Method of Covalent Attachment of Organic Functional Groups on Silica Gel, *J. Am.Chem. Soc.*, 2003, **125**, 4688-4689.

[43] Y. R. Yeon, Y. J. Park, J.S. Lee, J. W. Park, S.G. Kang and C.H. Jun, Sc(OTf)3-Mediated Silylation of Hydroxy Functional Groups on a Solid Surface: A Catalytic Grafting Method Operating at Room Temperature, *Angew. Chem. Int. Ed.*, 2008, **47**, 109-112.

[44] J. W. Park and C. H. Jun, Transition-Metal-Catalyzed Immobilization of Organic Functional Groups onto Solid Supports through Vinylsilane Coupling Reactions, *J. Am. Chem. Soc.*, 2010, **132**, 7268-7269.

[45] N. Moitra, S. Ichii, T. Kamei, K. Kanamori, Y. Zhu, K. Takeda, K. Nakanishi and T. Shimada, Surface Functionalization of Silica by Si–H Activation of Hydrosilanes, *J. Am. Chem. Soc.*, 2014,**136**, 11570−11573.

[46] N. Demirel, M. Merdivan, N. Pirinccioglu and C. Hamamci, Thorium(IV) and uranium(VI) sorption studies on octacarboxymethyl-C-methylcalix [4] resorcinarene impregnated on a polymeric support, *Anal. Chim. Acta*, 2003, **485**, 213–219.

[47] T. Yokoi, H. Yoshitake and T. Tatsumi, Synthesis of amino-functionalized MCM-41 via direct co-condensation and post-synthesis grafting methods using mono-, di- and tri-amino-organoalkoxysilanes, *J. Mater. Chem.*, 2004, **14**, 951–957.

[48] R.G. Parr and R.G. Pearson, Absolute hardness: companion parameter to absolute electronegativity *J. Am. Chem. Soc.*, 1983, **105**, 7512–7516.

[49] M. Tamada, N. Seko and F. Yoshii, Application of radiation-graft material for metal adsorbent and crosslinked natural polymer for healthcare product, *Radiat. Phys. Chem.*, 2004, **71**, 223-227.

[50] S. Zhang, P. Liu and B. Zhang, Thorium resources and their availability, *World Nucl. Geosci.*, 2005, **22**, 98-103.

[51] D. Humelnicu, G. Drochioiu, M.I. Sturza, A. Cecal and L.K. Popa, Kinetic and Thermodynamic aspects of U(IV) and Th(IV) sorption on a zeolitic volcanic tuff, *J. Radioanal. Nucl. Chem.*, 2006, **270,** 637-640.

[52] F. Basolo, R. G. Pearson, *Mechanism of inorganic reactions: A study of metal complexes in solution,* Wiley eastern Ltd., New York, 2nd Edition, 1977, 372-373.

[53] U. Chandra, O. Gilbert, B.E. K. Swamy, Y. D. Bodke and B.S. Sherigara, Electrochemical Studies of Eriochrome Black T at Carbon Paste Electrode and Immobilized by SDS Surfactant: A Cyclic Voltammetric Study, *Int. J. Electrochem. Sci.*, 2008, **3**, 1044-1054.

[54] Clayden, Greeves, Warren and Wothers, *Organic Chemistry*, Oxford University Press, Oxford,1st edition , 2001,597-600.

[55] J. Fan, C. Wu , Y. Wei, C. Peng and P. Peng, Preparation of xylenol orange functionalized silica gel as a selective solid phase extractor and its application for preconcentration separation of mercury from waters, *J. Hazard. Mater*., 2007, **145**, 323–330.

[56] C. K. Gupta and N. Krishnamurthy, *Extractive Metallurgy of Rare Earths*, CRC Press, Florida, 2nd Edition, 2004,310-312.

[57] F. A. Cotton, G. Wilkinson, C. A. Murilio and M. Bochmann, *Advanced Inorganic chemistry*; John Wiley & Sons , New York, 5th Edition, 1999, 604-605.

[58] K. Nakamoto, *Infrared and Raman spectra of Inorganic and Coordination compounds.Part B: Applications in Coordination, Organometallic, and Bioinorganic Chemistry*. John Wiley & Sons, New York, 5th edition, Sec.III 8, 1997, 59–62.

[59] E. Frisch, M. J. Frisch, F.R. Clemente Trucks, G. W.; Gaussian 09, Revision D.01.Gaussian, Inc., Wallingford CT, 2013.

[60] R. Argazzi, C. A. Bignozzi, T. A. Heimer, F. N. Castellano and G. J. Meyer, Long-Lived Photo-Induced Charge Separation Across Nanocrystalline TiO_2 Interfaces, *J. Am. Chem. Soc.*, 1995, **117**, 11815-11816.

[61] S. A. Haque, S. Handa, K. Peter, E. Palomares, M. Thelakkat and J. R. Durrant, Supermolecular Control of Charge Transfer in Dye-Sensitized Nanocrystalline TiO_2 Films: Towards a Quantitative Structure–Function Relationship , *Angew. Chem. Int. Ed.*, 2005, **44**, 5740 -5744.

[62] K. Hu, K. C. D. Robson, E. E. Beauvilliers, E. E. Schott, X. Zarate, R. A. Perez, C. P. Berlinguette and G. J. Meyer, Intramolecular- and Lateral Intermolecular-Hole Transfer at the Sensitized TiO_2 Interface, *J. Am. Chem. Soc.*, 2014, **136**, 1034-1046.

[63] B. Mandal, M. K. Barman and B. Srivastava, Extraction chromatographic method of preconcentration, estimation and concomitant separation of Vanadium (IV) with silica gel-Versatic 10 composite , *J. Chromatogr. Sci.*, 2014, **52**, 1135-1144.

[64] S. Ramakrishna, K. S. S. Kumar, D. Mathew and C. P. R. Nair, Long-living, stress- and pH-tolerant superhydrophobic silica particles via fast and efficient urethane chemistry; facile preparation of self recoverable SH coatings, *J. Mater. Chem. A*, 2015, **3**, 1465-1475.

[65] C.F. Baes and R.E. Mesmer, *The Hydrolysis of Cations*, John Wiley & Sons: Inc., New York, 1976 112-123.

[66] R. L. Ric, *Inorganic Reactions in Water*, 112 S. Spring St., Bluffton: USA, 2007, 65-74.

[67] N. Torapava, I. Persson, L. Eriksson and D. Lundberg, Hydration and Hydrolysis of Thorium(IV) in Aqueous Solution and the Structures of Two Crystalline Thorium(IV) Hydrates, *Inorg.Chem.* 2009, **48**, 11712-11723.

[68] D. L. Clark, D. E. Hobart and M. P. Neu, Actinide Carbonate Complexes and Their Importance in Actinide Environmental Chemistry, *Chem. Rev.*, 1995, **95**, 25-48.

[69] E. R. Davidson, K. L. Kunze, F. B. C. Machado and S. J. Chakravorty, The transition metal-carbonyl bond, *Ace. Chem. Res.*, 1993, **26**, 628-635.

[70] P. J. M. W. L. Birker, Stabilization of high oxidation states by strong electron-donating ligands. Crystal structure and properties of tetra-n-butylammonium o-phenylenebis (biuretato) cuprate(III)-chloroform,$(n\text{-}C_4H_9)_4NCu[o\text{-}C_6H_4(NCONHCONH)_2].CHCl_3$, *Inorg. Chem.*, 1977, **16**, 2478-2482.

[71] J. Xue-zhen, L. Hui-jun, W. Li-li, L. Jun, W. Yu-wen, L. Xiu-yun and Z. Xiao-jun, Adsorption of Thorium by Materials of β-Cyclodextrin Bonded Silica Gel, *J. Nucl. Radiochem.*, 2012, **1**, 40-45.

[72] A. Nilchi, T. S. Dehaghan and S. R. Garmarodi, Solid phase extraction of uranium and thorium on octadecyl bonded silica modified with Cyanex 302 from aqueous solutions, *J. Radioanal. Nucl. Chem.*, 2013, **295**, 2111-2115.

[73] S. Sadeghi and E. Sheikhzadeh, Solid phase extraction using silica gel functionalized with Sulfasalazine for preconcentration of uranium (VI) ions from water samples, *Microchim. Acta.*, 2008, **163**, 313-320.

[74] V.K. Jain, A. Honda, R. Pandya, P. Shirvastav and K.K. Agrawal, Polymer supported calyx [4]arene-semicarbazone derivative for separation and preconcentration of La(III), Ce(III), Th(IV) and U (VI), *React. Funct. Polym.* , 2002, **51**, 101-110.

[75] M. Shamsipur, Y. Yamini, P. Ashtari, A. R. Khanchi and M.G. Marageh, A Rapid Method for the Extraction and Separation of Uranium from Thorium and Other Accompanying Elements Using Octadecyl Silica Membrane Disks Modified by Tri-n-octyl Phosphine Oxide, *Sep. Sci. Technol.*, 2000, **35**, 1011-1019.

Mechanistic path 2a

synergistic attacment through donation and back donation operative on two different metal centers (Reaction condition: HOMO and LUMO of Resin (R) are at two different spatial locations)

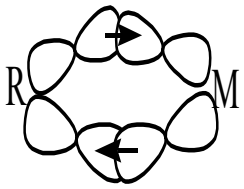

Mechanistic path 2b

synergistic attachment through donation and back donation operative on same metal center (Reaction condition:HOMO and LUMO of Resin (R) are both at the same spatial location

Scheme 2a *: FSG-EBT uniquely binds two metal centers,* Zr(IV)/U(VI)/Ti(IV) and Tl(I), in their high and low oxidation states simultaneously at its respective HOMO and LUMO which are spatially separated.

Scheme 2b*:* HOMO and LUMO are not spatially separated in ligand. Stabilization of high (by ligand like IO_6^{5-}) or low (by ligand like carbonyls) oxidation states of metals.

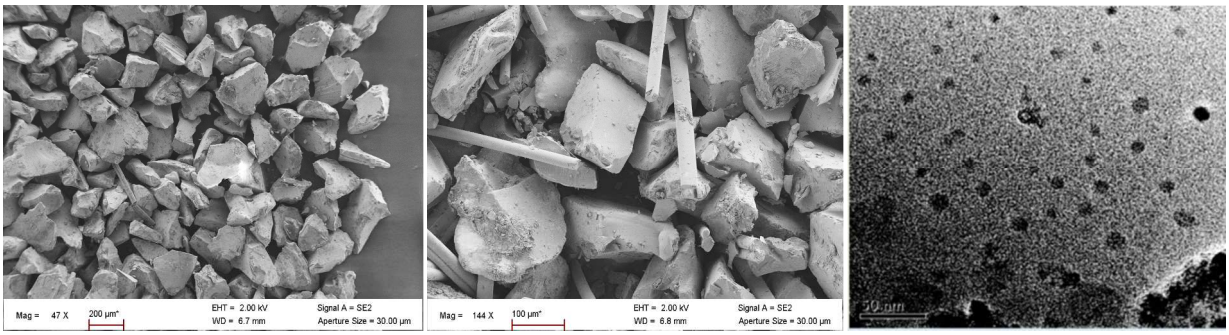

(a) (b) (c)

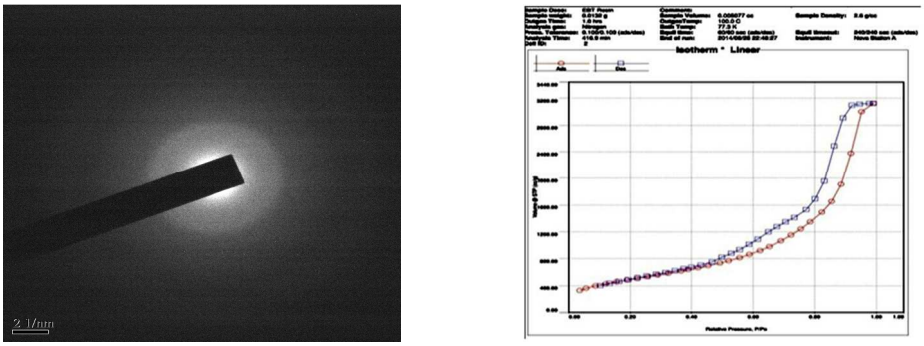

(d) (e)

Figure 1: SEM image of the ion-exchange material (a) free and (b) Th (IV) loaded; TEM & SEAD image of the corresponding nano material (c, d) and BET profile of the Resin (e)

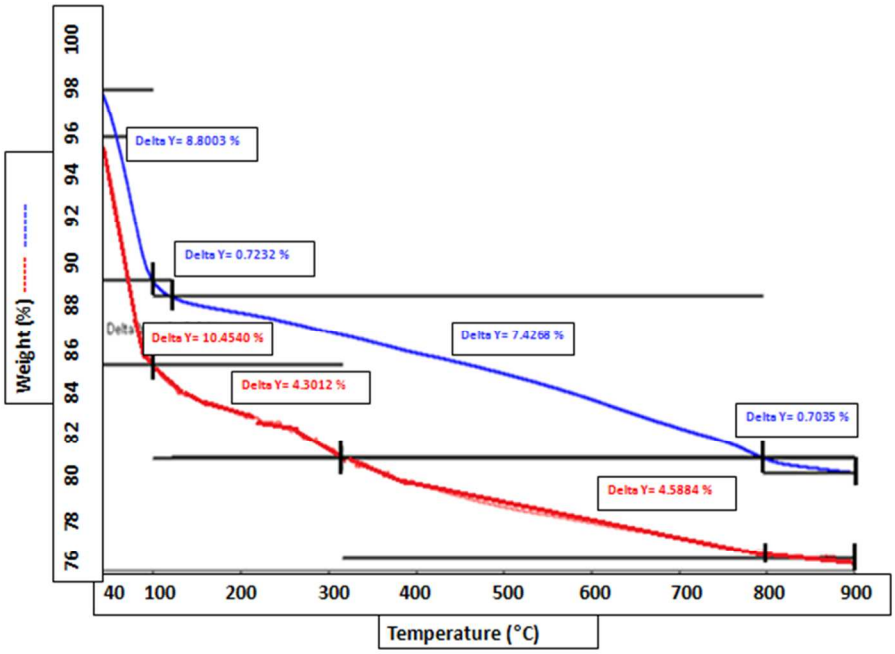

a

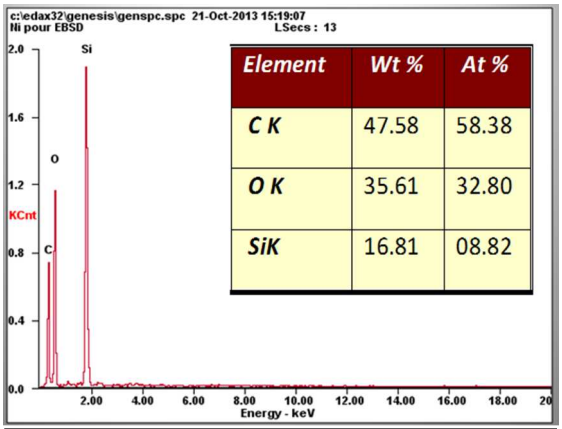

Element	Wt %	At %
C K	47.58	58.38
O K	35.61	32.80
SiK	16.81	08.82

(b)

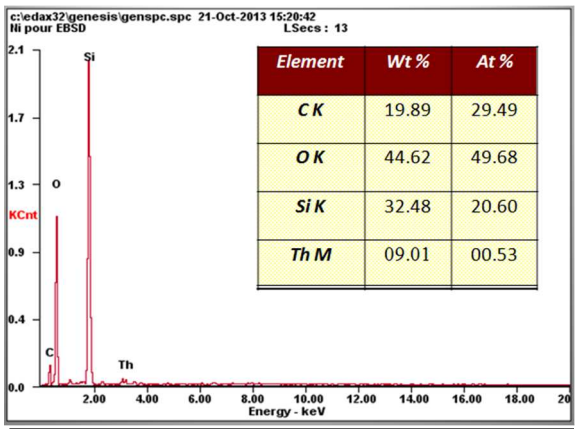

Element	Wt %	At %
C K	19.89	29.49
O K	44.62	49.68
Si K	32.48	20.60
Th M	09.01	00.53

(c)

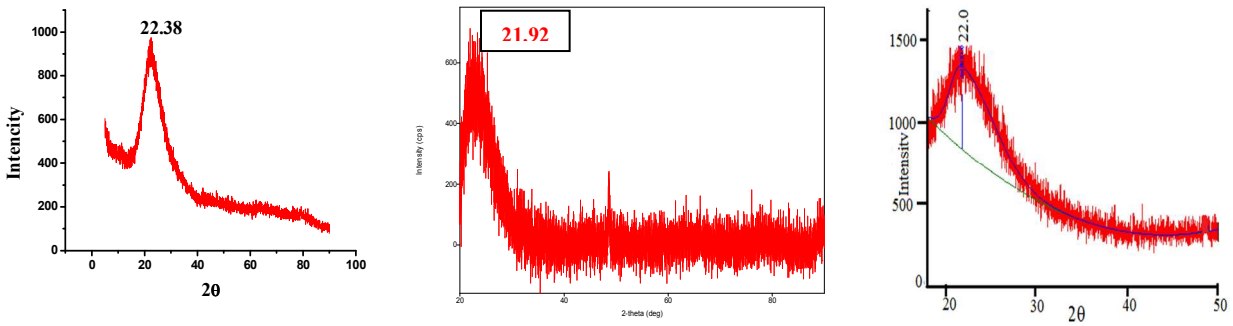

(d) (e) (f)

Figure 2: TGA analysis of FSG-EBT: (a) TGA curve of the extractor (upper curve) and TGA curve of the Th (IV) loaded extractor; (b) EDX spectra of the extractor and extractor -Th(IV) complex. (c) XRD spectra of the synthesized resin (e) XRD spectra of the Zr (IV) and Tl(I) loaded extractor (2θ: 21.92) and (f) XRD spectra of the silica gel.

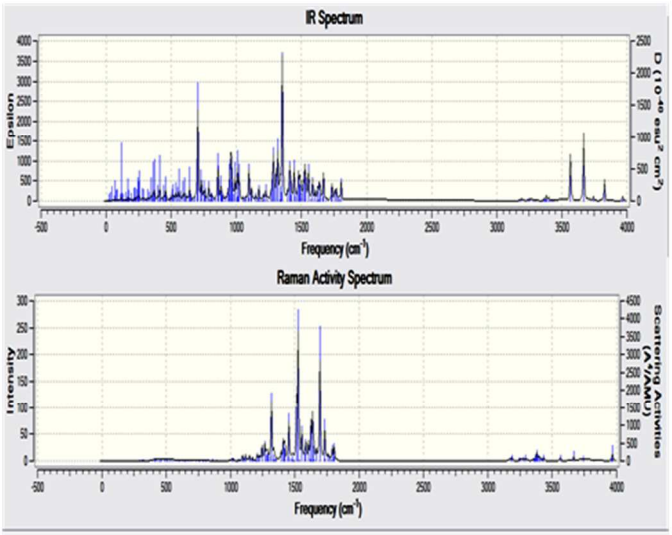

(a)

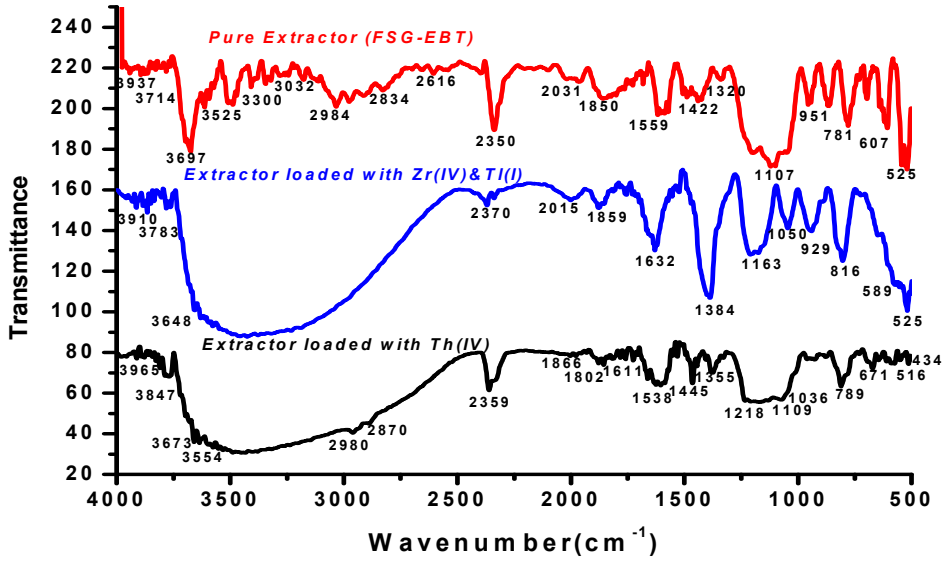

(b)

Figure 3: FT-IR spectra (a) FT-IR and RAMAN spectra of DFT optimized structure of FSG-EBT; (b) experimental FT-IR spectra (upper curve corresponds to the Th-loaded extractor while lower curve corresponds to the unloaded extractor)

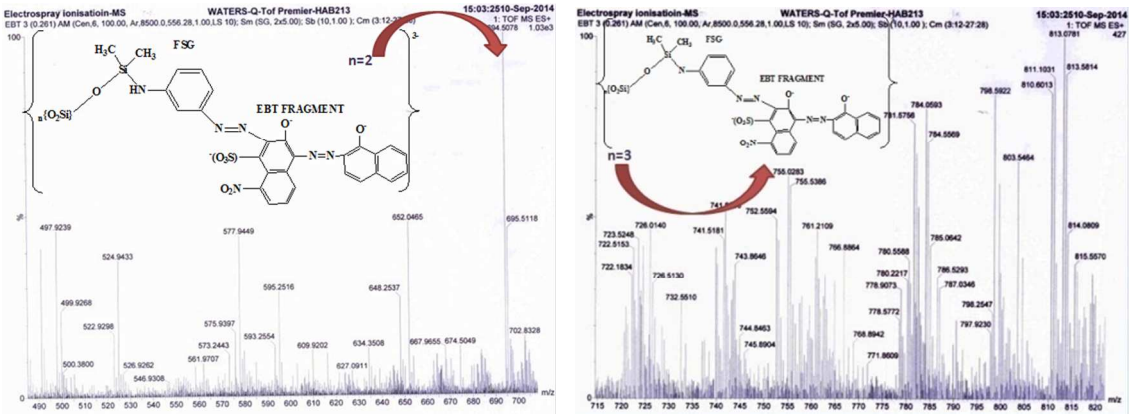

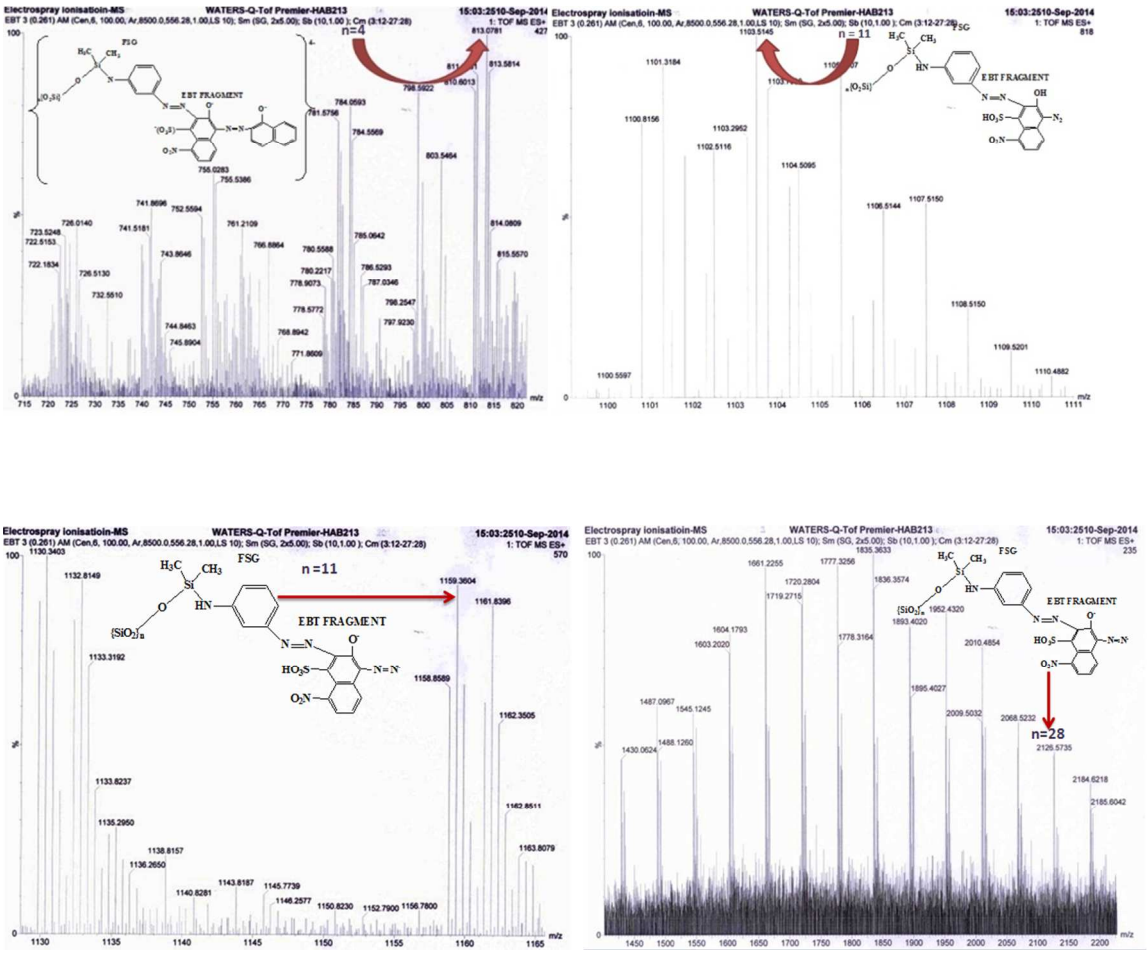

Figure 4: An electrospray ionization-Tof-derived mass spectrum of the synthesized extractor (a-f)

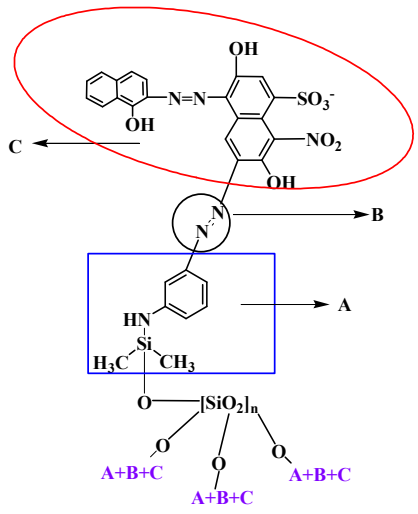

Two dimentional structure of FSG-EBT

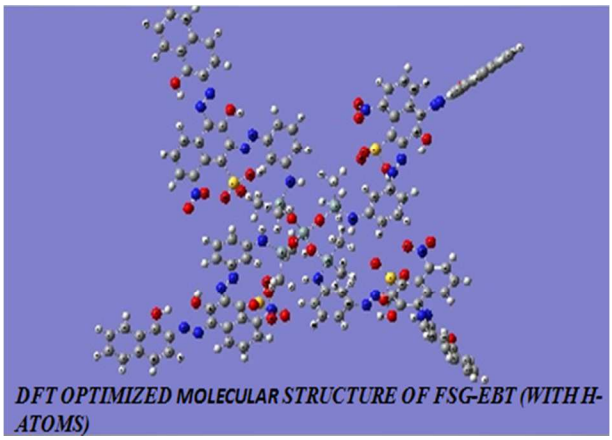

DFT OPTIMIZED MOLECULAR STRUCTURE OF FSG-EBT (WITH H-ATOMS)

(a) (b)

Figure 5: (a) 2D structure of FSG-EBT (b) DFT optimized molecular structure of FSG-EBT

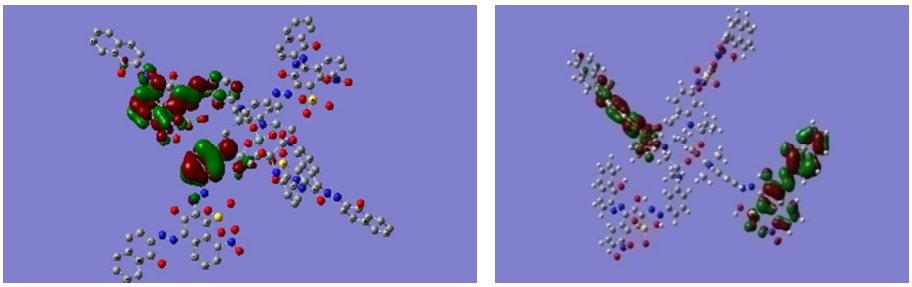

(a) **(b)**

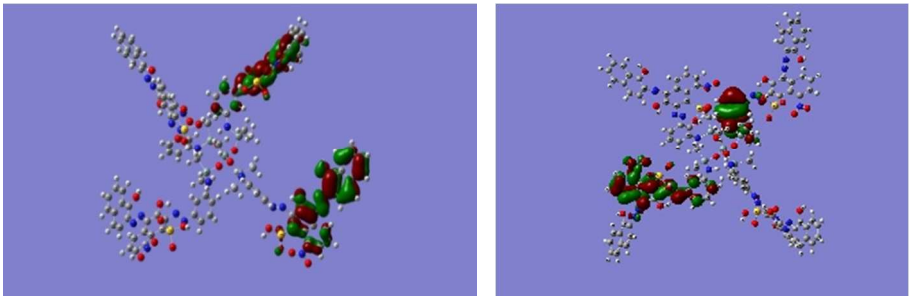

(c) **(d)**

Figure 6: Spatial positions of HOMO and LUMO at different time interval ($\eta_{\text{FSG-EBT}}$ = 9.0106 eV; Dipole moment: 8.3613 Debye (a-e)

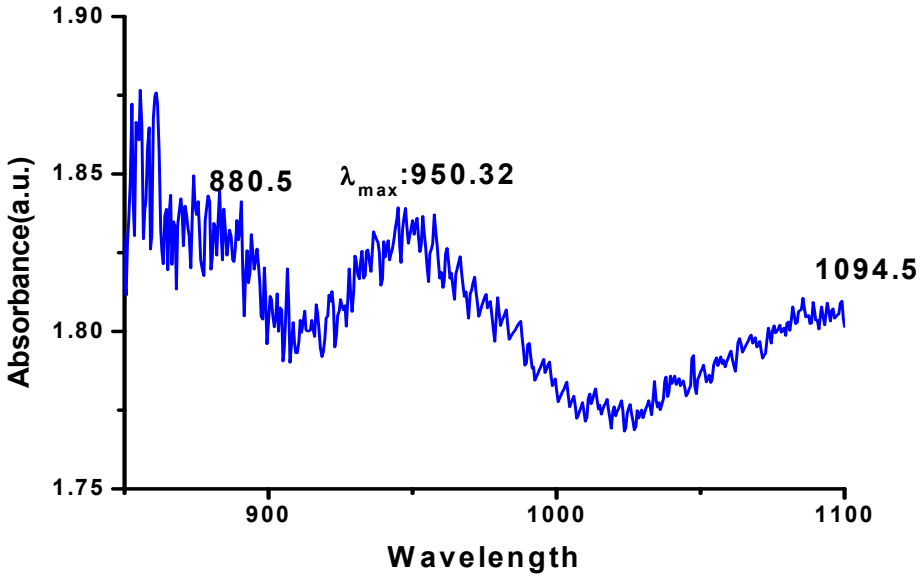

(a)

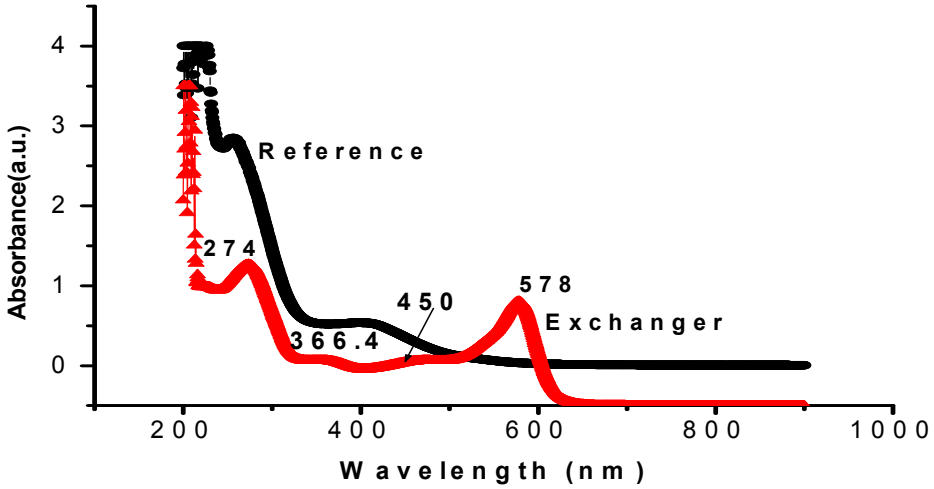

(b)

Figure 7: UV-visible spectra of the extractor-Th (IV) complex at different mole ratio (a-b).

(a) (b)

Figure 8: Effect of pH on (a) Extraction and (b) Conductance of aqueous Th (IV) solution.

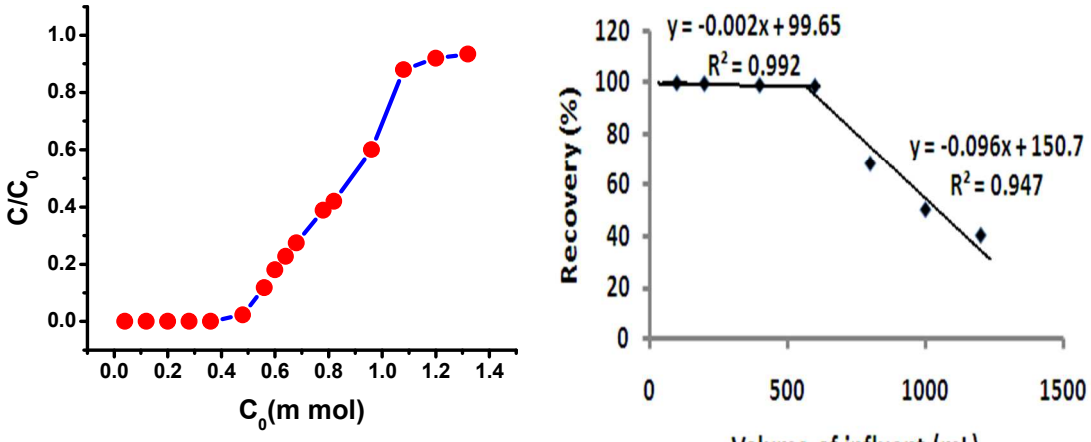

(a) (b)

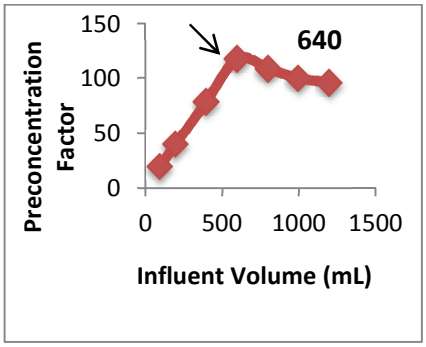

(c)

Figure 9: (a) Break-through curve; (b) Plot of Volume of influent vs. Recovery (%) (c) Plot of influent volume vs. Preconcentration factor

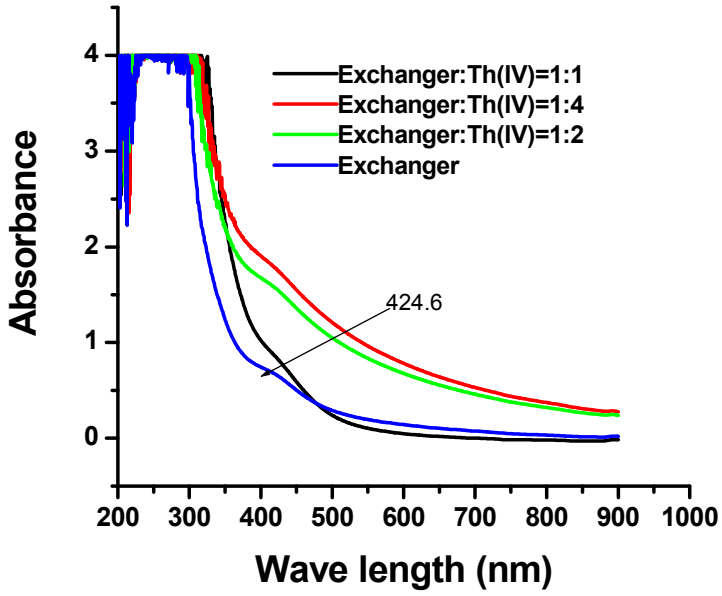

Figure 10: UV-Visible spectrum of the extractor (a, b) experimental upper curve corresponds to EBT and lower curve corresponds to EBT-Th (IV) complex

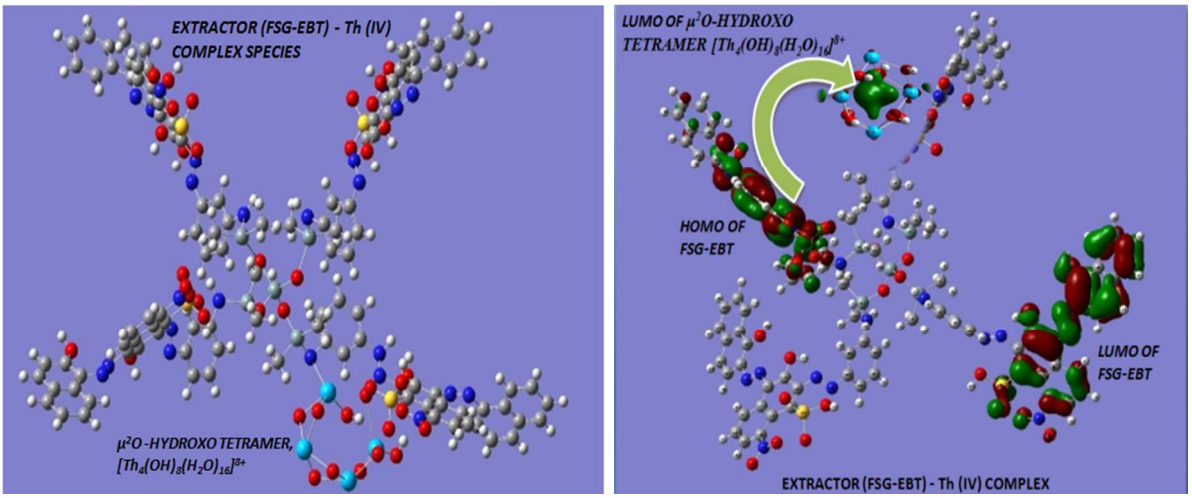

(a) (b)

Figure 11: Extractor-Th (IV) complex species (a) μ^2*O*-hydroxo tetramer, $[Th_4(OH)_8(H_2O)_{16}]^{8+}$ (b) Th(IV) exists as its tetramer in the vicinity of HOMO in extractor -metal complex.

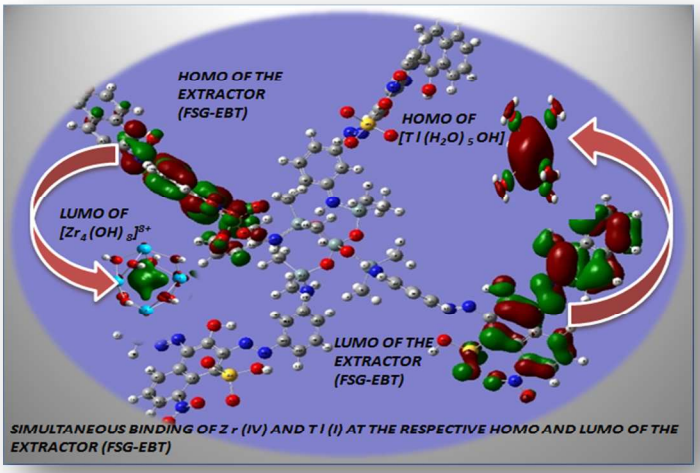

Figure 12: Simultaneous binding of Zr (IV) and Tl(I) at the respective HOMO and LUMO of the extractor(FSG-EBT) : Donation of electron cloud from HOMO of extractor to LUMO of the zirconium species and back donation of electron cloud from HOMO of thallium species to LUMO of the extractor

Table 1: ***Effect of interfering cations/anions on extraction of Th(IV);*** [Column = 0.8x8 cm.; Th(IV) taken = 3.48 mg ; Flow-rate =1.0 mL min^{-1}; pH = 6.5; Sample volume = 50 mL]

Interfering ion	**Interfering ion ([a]µg (50-300)/ [b]µg (0.025-0.25)/ Retention (%))**					
	50/0.025	100/0.05	150/0.125	200/0.175	250/0.20	300/0.25
[a]Cl^-	99.2	98.8	98.6	98.1	**97.2 (0.028)** *	96.2
[a]SO_4^{2-}	98.5	97.2	96.1	94.9	**92.1 (0.042)** *	87.6
[a]ClO_4^-	99.1	98.7	97.3	97.1	**96.2(0.025)** *	89.5
[a]NO_3^-	99.4	99.1	98.5	98.4	**97.6(0.033)** *	91.4
[a]CH_3COO^-	99.7	99.6	99.2	98.5	**98.0 (0.041)** *	97.4
[a]Na(I)	99.4	98.8	98.6	98.3	**97.2 (0.035)** *	96.2
[a]K(I)	99.1	98.6	98.2	97.7	**97.2 (0.038)** *	96.2
[a]Mg(II)	98.2	95.4	93.7	92.4	**91.1 (0.032)** *	90.2
[a]Ca(II)	97.8	95.6	94.2	92.1	**90.7 (0.029)** *	78.4
[a]Zn(II)	98.5	97.2	95.5	93.7	**92.0 (0.035)** *	87.9
[a]Ni(II)	99.2	97.6	95.7	93.2	**90.5 (0.042)** *	88.2
[b]La(III)	99.5	98.2	97.3	95.0	**94.7 (0.048)** *	94.0
[b]Ce(IV)	98.0	97.0	96.1	93.6	**92.2 (0.039)** *	91.4
[b]Dy(III)	99.2	98.4	97.0	95.2	**94.3 (0.032)** *	93.6
[b]Eu(III)	99.0	97.3	96.1	94.3	**92.8 (0.036)** *	91.6

* **Average of 5 determinations: SD are given in parenthesis**

Table 2: Elution study of Th (IV)

[Th (IV) taken: 3.94 mg; Column-0.8×8cm; flow rate: 1mL min^{-1}, pH: 7.0 ± 0.5; temp: 25^0C]

Eluent	**Conc.(mol L^{-1})×10^3**	**V_{max} (mL)**	**V_{total} (mL)**	**#Recovery (%)**
HNO_3	10	15	**30**	96.6
	100	12	20	96.7
	200	8	18	97.0
	300	10	15	98.2
	400	15	20	98.6
	500	8	20	98.8
	1000	15	25	98.9
HCl	5.00	--	---	Nil
	10.0	9	20	98.2
	100	16	28	99.6
H_2SO_4	1.25	12	30	96.2
	2.50	12	28	98.4
	5.00	14	20	98.8
	10.0	10	20	98.9
	200.0	8	18	99.1
CH_3COOH	5-30	--	--	--
	50	12	25	**97.2**
	100	9	**25**	**98.6**
	200	15	**40**	**98.8**

$HClO_4$	0.6	12	25	97.3
	1.25	12	20	97.9
	2.5	10	20	96.8
	5.0	9	20	98.9
	10.0	8	20	99.1
	100	8	20	99.6
	500	2.5	5	99.8

[#]Average of five determinations

Table 3: Comparison of the synthesized material with previously published literature.

Silica Gel imprinted sorbents	Synthesis condition (time period of whole synthesis)	Metals studied	pH and Flow-rate (mL min^{-1})	BET surface area (m^2g^{-1})	PF/ Eluent used	Break through capacity ($\mu M\, g^{-1}$)	Spatial Separation of HOMO-LUMO	Ref.
Eriochrome black T	1h	Th(IV) Zr(IV) U(VI) Tl(I)	6.5-7.5 And 2.0	330.968	120.20 ± 0.04/0.1 mol L^{-1} HNO_3	498	Yes Yes	This work
Versatic-10	20 h	Ti(IV)	5.0-6.0 and 2.5	149.46	60.8 ± 0.5, (1 mol L^{-1} HCl)	37.4-40.7	--- ---	[27]

CPMA –PMASG composite	64 h	Th(IV)	2.5-5.0 And 1-12	125	3mol L^{-1} HCl	43	--- ---	[36]
β-Cyclodextrin	4 h	Th(IV)	2.0-3.0 And 5.0	---	25,---	336.1	--- ---	[71]
Cyanex 302	28 h	Th(IV) U(VI)	6.0 And 7.0	---	30,(Cyanex 302 in 2mL methanol)	129.2	--- ---	[72]
Sulfasalazine	75 h	Th(IV) U(VI)	5.5 And 10	---	400,(0.1 $molL^{-1}$ HCl)	97.8±0.	--- ---	[73]
Calix (4)arenearene semi-carbazone	54 h	Th(IV) La(III) Ce(III) U(VI)	2.5–4.5 And 2.0	127	102,(0.01 mol L^{-1} HCl,2.0 mol L^{-1} HCl)	100	--- ---	[74]
Tri-n-octyl Phosphine Oxide	1h	Th(IV) U(VI)	8.35 And 2.0	---	165,(0.5–1 mol L^{-1} HNO_3, 0.5 mol L^{-1} HCl.)	---	--- ---	[75]

Table 4: Break-through capacity (BTC) of different extractors and its correlation with the amount of HOMO/LUMO (µmol g^{-1}) (3FSG: 1, 3 nitro aniline is used to synthesize FSG; 4FSG: 1, 4 nitro aniline is used to synthesize FSG; 2 methyl-3FSG: 2-methyl-1, 3 nitro aniline is used to synthesize FSG)

Different FSG-X	**Mol. Wt. (g)**	**Amount of HOMO/LUMO (= *x* µmol g^{-1})**	**Exp. BTC (µmol g^{-1})[M]**	**No. of metal trapping groups**	**BTC = q×[HOMO or LUMO] (µmol g^{-1})**
***3*FSG-EBBBB** **EBBBB = Eriochrome Blue Black B**	7379	135.5	508 [Th(IV)]	Two – OH(phenolic) one –N=N- one $–SO_3H$	(q=4)× x
			496 [Zr(IV)]		(q=4) × x
			502 [U(VI)]		(q=4)× *x*
			260 [Ti(IV)]		(q=2)× *x*
***3*FSG-EBT** **EBT = Eriochrome Black T**	7563	132.2	518 [Th(IV)]	Two – OH(phenolic) one –N=N- one $–SO_3H$ one $–NO_2$	(q=4)× *x*
			490 [Zr(IV)]		(q=4)× *x*
			522 [U(VI)]		(q=4)× *x*
			252 [Ti(IV)]		(q=2)× *x*
***3*FSG-GNV**	4994.32	200.2	769 [Th(IV)]	One –OH (phenolic) one -COOH	(q=4)× *x*
			779 [Zr(IV)]		(q=4)× *x*
			762 [U(VI)]		(q=4)× *x*

			375 [Ti(IV)]	one –N=N- one-NHR	(q=2)× *x*
***4*FSG-EBBBB** **EBBBB = Eriochrome Blue Black B**	7379	135.5	517 [Th(IV)]	Two – OH(phenolic) one –N=N- one –SO_3H	(q=4)× *x*
			510 [Zr(IV)]		(q=4)× *x*
			521 [U(VI)		(q=4)× *x*
			246 [Ti(IV)]		(q=2)× *x*
***4*FSG-EBT** **EBT = Eriochrome Black T**	7563	132.2	512 [Th(IV)]	Two – OH(phenolic) one –N=N- one –SO_3H one-NO_2	(q=4)× *x*
			496 [Zr(IV)]		(q=4)× *x*
			523 [U(VI)		(q=4)× *x*
			244 [Ti(IV)]		(q=2)× *x*
***4*FSG-GNV**	4994.32	200.2	775 [Th(IV)]	One –OH (phenolic) one -COOH one – N=N- one-NHR	(q=4)× *x*
			787 [Zr(IV)]		(q=4)× *x*
			798 [U(VI)		(q=4)× *x*
			372 [Ti(IV)]		(q=2)× *x*
***2 methyl-3*FSG-PAN**	4287.4	233.2	898 [Cd(II)]	One – OH(phenolic) One N(pyridyl)	(q=4)× *x*
			907 [Zn(II)]		(q=4)× *x*
			902 [Hg(II)		(q=4)× *x*

			415 [Ti(IV)]	one –N=N-	(q=2)× *x*
***2 methyl 3*FSG-NV**	5138.32	194.6	724 [Cd(II)]	One – OH(phenolic) two -COOH one –N=N-	(q=4)× *x*
			730 [Zn(II)]		(q=4)× *x*
			715 [Hg(II)		(q=4)× *x*
			369 [Ti(IV)]		(q=2)× *x*
***2 methyl 3*FSG-GNV**	5054.32	197.8	733 [Cd(II)]	One –OH (phenolic) one -COOH one –N=N-one-NHR	(q=4)× *x*
			740 [Zn(II)]		(q=1)× *x*
			716 [Hg(II)		(q=1)× *x*
			370 [Ti(IV)]		(q=2)× *x*

For Table of Contents Only

TOC graphic and synopsis

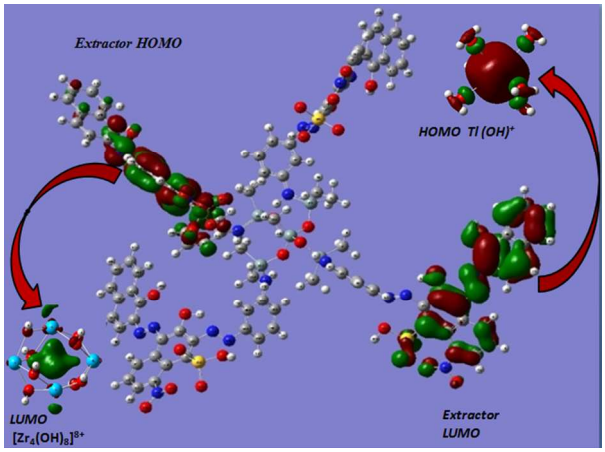

Simultaneous binding of two different metal centers, Zr(IV) and Tl(I) at the respective HOMO and LUMO of the extractor (FSG-EBT)

Graphical Abstract

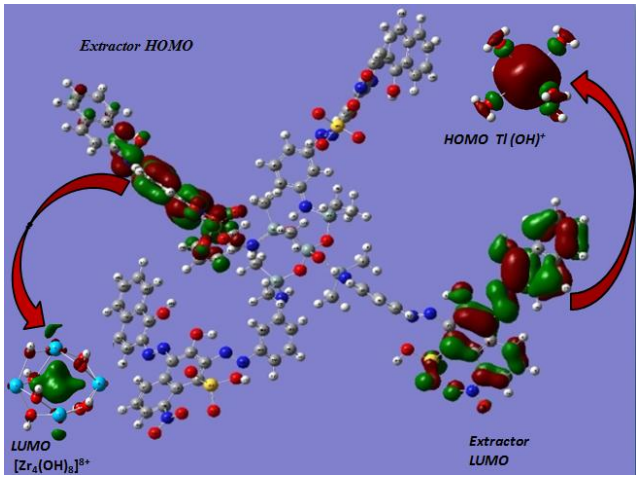

Simultaneous binding of two different metal centers, Zr (IV) and Tl (I) at the respective HOMO and LUMO of the extractor (FSG-EBT)